

Fundamental limits on the rate of bacterial cell division

³ **Nathan M. Belliveau^{†, 1}, Griffin Chure^{†, 2, 3}, Christina L. Hueschen⁴, Hernan G.
⁴ Garcia⁵, Jané Kondev⁶, Daniel S. Fisher⁷, Julie Theriot^{1, 8}, Rob Phillips^{2, 9, *}**

*For correspondence:

[†]These authors contributed equally to this work

⁵ ¹Department of Biology, University of Washington, Seattle, WA, USA; ²Division of
⁶ Biology and Biological Engineering, California Institute of Technology, Pasadena, CA,
⁷ USA; ³Department of Applied Physics, California Institute of Technology, Pasadena, CA,
⁸ USA; ⁴Department of Chemical Engineering, Stanford University, Stanford, CA, USA;
⁹ ⁵Department of Molecular Cell Biology and Department of Physics, University of
¹⁰ California Berkeley, Berkeley, CA, USA; ⁶Department of Physics, Brandeis University,
¹¹ Waltham, MA, USA; ⁷Department of Applied Physics, Stanford University, Stanford, CA,
¹² USA; ⁸Allen Institute for Cell Science, Seattle, WA, USA; ⁹Department of Physics,
¹³ California Institute of Technology, Pasadena, CA, USA; *Contributed equally

¹⁴

¹⁵ **Abstract** This will be written next

¹⁶

¹⁷ Introduction

¹⁸ The range of bacterial growth rates is enormously diverse. In natural environments, some micro-
¹⁹ bial organisms might double only once per year while in comfortable laboratory conditions, growth
²⁰ can be rapid with several divisions per hour. This six order of magnitude difference illustrates the
²¹ intimate relationship between environmental conditions and the rates at which cells convert nu-
²² trients into new cellular material – a relationship that has remained a major topic of inquiry in
²³ bacterial physiology for over a century (*Jun et al., 2018*). As was noted by Jacques Monod, “the
²⁴ study of the growth of bacterial cultures does not constitute a specialized subject or branch of re-
²⁵ search, it is the basic method of Microbiology.” Those words ring as true today as they did when
²⁶ they were written 70 years ago. Indeed, the study of bacterial growth has undergone a molecular
²⁷ resurgence since many of the key questions addressed by the pioneering efforts in the middle of
²⁸ the last century can be revisited by examining them through the lens of the increasingly refined
²⁹ molecular census that is available for bacteria such as the microbial workhorse *Escherichia coli*. Sev-
³⁰ eral of the outstanding questions that can now be studied about bacterial growth include: what
³¹ sets the fastest time scale that bacteria can divide, and how is growth rate tied to the quality of the
³² carbon source. In this paper, we address these two questions from two distinct angles. First, as
³³ a result of an array of high-quality proteome-wide measurements of the *E. coli* proteome under a
³⁴ myriad of different growth conditions, we have a census that allows us to explore how the num-
³⁵ ber of key molecular players change as a function of growth rate. This census provides a window
³⁶ onto whether the processes they mediate such as molecular transport into the cells and molecular
³⁷ synthesis within cells can run faster. Second, because of our understanding of the molecular path-
³⁸ ways responsible for many of the steps in bacterial growth, we can also make order of magnitude
³⁹ estimates to infer the copy numbers that would be needed to achieve a given growth rate. In this
⁴⁰ paper, we pass back and forth between the analysis of a variety of different proteomic datasets and
⁴¹ order-of-magnitude estimations to determine possible molecular bottlenecks that limit bacterial

42 growth and to see how the growth rate varies in different carbon sources.

43 Specifically, we leverage a combination of *E. coli* proteomic data sets collected over the past
 44 decade using either mass spectrometry (*Schmidt et al., 2016; Peebo et al., 2015; Valgepea et al.,
 45 2013*) or ribosomal profiling (*Li et al., 2014*) across 31 unique growth conditions. Broadly speaking,
 46 we entertain several classes of hypotheses as are illustrated in **Figure 1**. First, we consider potential
 47 limits on the transport of nutrients into the cell. We address this hypothesis by performing an
 48 order-of-magnitude estimate for how many carbon, phosphorous, and sulfur atoms are needed to
 49 facilitate this requirement given a 5000 second division time. As a second hypothesis, we consider
 50 the possibility that there exists a fundamental limit on how quickly the cell can generate ATP. We
 51 approach this hypothesis from two angles, considering how many ATP synthase complexes must
 52 be needed to churn out enough ATP to power protein translation followed by an estimation of
 53 how many electron transport complexes must be present to maintain the proton motive force.
 54 A third class of estimates considers the need to maintain the size and shape of the cell through
 55 the construction of new lipids for the cell membranes as well as the glycan polymers which make
 56 up the rigid peptidoglycan. Our final class of hypotheses centers on the synthesis of a variety of
 57 biomolecules. Our focus is primarily on the stages of the central dogma as we estimate the number
 58 of protein complexes needed for DNA replication, transcription, and protein translation.

59 In broad terms, we find that the majority of these estimates are in close agreement with the
 60 experimental observations, with protein copy numbers apparently well-tuned for the task of cell
 61 doubling. This allows us to systematically scratch off the hypotheses diagrammed in **Figure 1** as
 62 setting possible speed limits. Ultimately, we find that protein translation (particularly the genera-
 63 tion of new ribosomes) acts as 1) a rate limiting step for the *fastest* bacterial division, and 2) the
 64 major determinant of bacterial growth across all nutrient conditions we have considered under
 65 steady state, exponential growth. This perspective is in line with the linear correlation observed
 66 between growth rate and ribosomal content (typically quantified through the ratio of RNA to pro-
 67 tein) for fast growing cells (*Scott et al., 2010*), but suggests a more prominent role for ribosomes
 68 in setting the doubling time across all conditions of nutrient limitation. Here we again leverage the
 69 quantitative nature of this data set and present a quantitative model of the relationship between
 70 the fraction of the proteome devoted to ribosomes and the speed limit of translation, revealing
 71 a fundamental tradeoff between the translation capacity of the ribosome pool and the maximal
 72 growth rate.

73 Uptake of Nutrients

74 In order to build new cellular mass, the molecular and elemental building blocks must be scav-
 75 enged from the environment in different forms. Carbon, for example, is acquired via the transport
 76 of carbohydrates and sugar alcohols with some carbon sources receiving preferential treatment
 77 in their consumption (*Monod, 1947*). Phosphorus, sulfur, and nitrogen, on the other hand, are har-
 78 vested primarily in the forms of inorganic salts, namely phosphate, sulfate, and ammonia (*Jun et al.,
 79 2018; Assentoft et al., 2016; Stasi et al., 2019; Antonenko et al., 1997; Rosenberg et al., 1977; Will-
 80 sky et al., 1973*). All of these compounds have different permeabilities across the cell membrane
 81 (*Phillips 2018*) and most require some energetic investment either via ATP hydrolysis or through
 82 the proton electrochemical gradient to bring the material across the hydrophobic cell membrane.
 83 Given the diversity of biological transport mechanisms and the vast number of inputs needed to
 84 build a cell, we begin by considering transport of some of the most important cellular ingredients:
 85 carbon, nitrogen, oxygen, hydrogen, phosphorus, and sulfur.

86 The elemental composition of *E. coli* has received much quantitative attention over the past
 87 half century (*Neidhardt et al., 1991; Taymaz-Nikerel et al., 2010; Heldal et al., 1985; Bauer and
 88 Ziv, 1976*), providing us with a starting point for estimating the copy numbers of various trans-
 89 porters. While there is some variability in the exact elemental percentages (with different uncer-
 90 tainties), we can estimate that the dry mass of a typical *E. coli* cell is \approx 45% carbon (BNID: 100649,
 91 *Milo et al. (2010)*), \approx 15% nitrogen (BNID: 106666, *Milo et al. (2010)*), \approx 3% phosphorus (BNID:

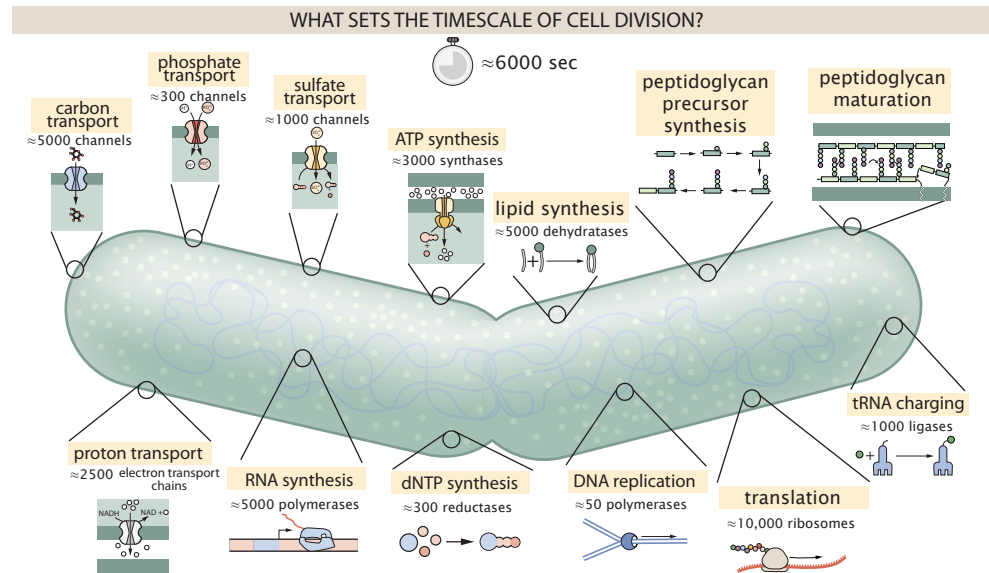


Figure 1. Transport and synthesis processes necessary for cell division. We consider an array of processes necessary for a cell to double its molecular components. Such processes include the transport of carbon across the cell membrane, the production of ATP, and fundamental processes of the central dogma namely RNA, DNA, and protein synthesis. A schematic of each synthetic or transport category is shown with an approximate measure of the complex abundance at a growth rate of 0.5 per hour. In this work, we consider a standard bacterial division time of ≈ 5000 sec.

92 100653, *Milo et al. (2010)*), and 1% sulfur (BNID: 100655, *Milo et al. (2010)*). In the coming para-
 93 graphs, we will engage in a dialogue between back-of-the-envelope estimates for the numbers of
 94 transporters needed to facilitate these chemical stoichiometries and the experimental proteomic
 95 measurements of the biological reality. Such an approach provides the opportunity to test if our
 96 biological knowledge is sufficient to understand the scale at which these complexes are produced.
 97 Specifically, we will make these estimates considering a modest doubling time of 5000 s, a growth
 98 rate of $\approx 0.5 \text{ hr}^{-1}$, the range in which the majority of the experimental measurements reside.

99 Nitrogen Transport

100 Before we begin our back-of-the-envelope estimations, we must address which elemental sources
 101 must require proteinaceous transport, meaning that the cell cannot acquire appreciable amounts
 102 simply via diffusion from the membrane. The permeability of the lipid membrane to a large num-
 103 ber of solutes has been extensively characterized over the past century. Large, polar molecular
 104 species (such as various sugar molecules, sulfate, and phosphate) have low permeabilities while
 105 small, non-polar compounds (such as oxygen, carbon dioxide, and ammonia) can readily diffuse
 106 across the membrane. Ammonia, a primary source of nitrogen in typical laboratory conditions,
 107 has a permeability on par with water ($\approx 10^5 \text{ nm/s}$, BNID:110824 *Milo et al. (2010)*). In particularly
 108 nitrogen-poor conditions, *E. coli* expresses a transporter (AmtB) which appears to aid in nitrogen
 109 assimilation, though the mechanism and kinetic details of transport is still a matter of debate (*van*
 110 *Heeswijk et al., 2013; Khademi et al., 2004*). Beyond ammonia, another plentiful source of nitrogen
 111 come in the form of glutamate, which has its own complex metabolism and scavenging pathways.
 112 However, nitrogen is plentiful in the growth conditions examined in this work, permitting us to ne-
 113 glect nitrogen transport as a potential rate limiting process in cell division in typical experimental
 114 conditions. We direct the reader to the supplemental information for a more in-depth discussion of
 115 permeabilities and a series of calculations revealing that active nitrogen transport can be neglected
 116 for the purposes of this article.

117 **Carbon Transport**

118 We begin our estimations with the most abundant element in *E. coli* by mass, carbon. Using ≈ 0.3
 119 pg as the typical *E. coli* dry mass (BNID: 103904, *Milo et al. (2010)*), we estimate that $\approx 10^{10}$ carbon
 120 atoms must be brought into the cell in order to double all of the carbon-containing molecules (*Fig-*
 121 *ure 2(A, top)*). Typical laboratory growth conditions, such as those explored in the aforementioned
 122 proteomic data sets, provide carbon as a single class of sugar such as glucose, galactose, or xylose
 123 to name a few. *E. coli* has evolved myriad mechanisms by which these sugars can be transported
 124 across the cell membrane. One such mechanism of transport is via the PTS system which is a
 125 highly modular system capable of transporting a diverse range of sugars (*Escalante et al., 2012*).
 126 The glucose-specific component of this system transports ≈ 200 glucose molecules per second per
 127 transporter (BNID: 114686, *Milo et al. (2010)*). Making the assumption that this is a typical sugar
 128 transport rate, coupled with the need to transport 10^{10} carbon atoms, we arrive at the conclusion
 129 that on the order of 1,000 transporters must be expressed in order to bring in enough carbon
 130 atoms to divide in 5000 s, diagrammed in the top panel of *Figure 2(A)*. This estimate, along with
 131 the observed average number of the PTS system carbohydrate transporters present in the pro-
 132 teomic data sets (*Schmidt et al., 2016; Peebo et al., 2015; Valgepea et al., 2013; Li et al., 2014*), is
 133 shown in *Figure 2(A)*. While we estimate 1500 transporters are needed with a 5000 s division time,
 134 we can abstract this calculation to consider any particular growth rate given knowledge of the cell
 135 density and volume as a function of growth rate and direct the reader to the SI for more informa-
 136 tion. As revealed in *Figure 2(A)*, experimental measurements exceed the estimate by several fold,
 137 illustrating that transport of carbon in to the cell is not rate limiting for cell division. Abstracting
 138 this point estimate at 5000 s to a continuum of growth rates (grey line in *Figure 2(A)*) reveals an
 139 excess of transporters at other growth rates, though in rapid growth regimes, the abundance is
 140 below our simple estimate.

141 The estimate presented in *Figure 2(A)* neglects any specifics of the regulation of carbon trans-
 142 port system and presents a data-averaged view of how many carbohydrate transporters are present
 143 on average. Using the diverse array of growth conditions explored in the proteomic data sets, we
 144 can explore how individual carbon transport systems depend on the population growth rate. In
 145 *Figure 2(B)*, we show the total number of carbohydrate transporters specific to different carbon
 146 sources. A striking observation, shown in the top-left plot of *Figure 2(B)*, is the constancy in the
 147 expression of the glucose-specific transport systems. Additionally, we note that the total number
 148 of glucose-specific transporters is tightly distributed $\approx 10^4$ per cell, the approximate number of
 149 transporters needed to sustain rapid growth of several divisions per hour. This illustrates that *E.*
 150 *coli* maintains a substantial number of complexes present for transporting glucose which is known
 151 to be the preferential carbon source (*Monod, 1947; Liu et al., 2005; Aidelberg et al., 2014*).

152 It is now understood that a large number of metabolic operons are regulated with dual-input
 153 logic gates that are only expressed when glucose concentrations are low (mediated by cyclic-AMP
 154 receptor protein CRP) and the concentration of other carbon sources are elevated (*Gama-Castro*
et al., 2016; Zhang et al., 2014b). A famed example of such dual-input regulatory logic is in the regu-
 155 lation of the *lac* operon which is only natively activated in the absence of glucose and the presence
 156 of allolactose, an intermediate in lactose metabolism (*Jacob and Monod, 1961*), though we now
 157 know of many other such examples (*Ireland et al., 2020; Gama-Castro et al., 2016; Belliveau et al.,*
 158 *2018*). This illustrates that once glucose is depleted from the environment, cells have a means to
 159 dramatically increase the abundance of the specific transporter needed to digest the next sugar
 160 that is present. Several examples of induced expression of specific carbon-source transporters
 161 are shown in *Figure 2(B)*. Points colored in red (labeled by red text-boxes) correspond to growth
 162 conditions in which the specific carbon source (glycerol, xylose, or fructose) is present. These plots
 163 show that, in the absence of the particular carbon source, expression of the transporters is main-
 164 tained on the order of $\sim 10^2$ per cell. However, when the transport substrate is present, expression
 165 is induced and the transporters become highly-expressed. The grey lines in *Figure 2(B)* show the

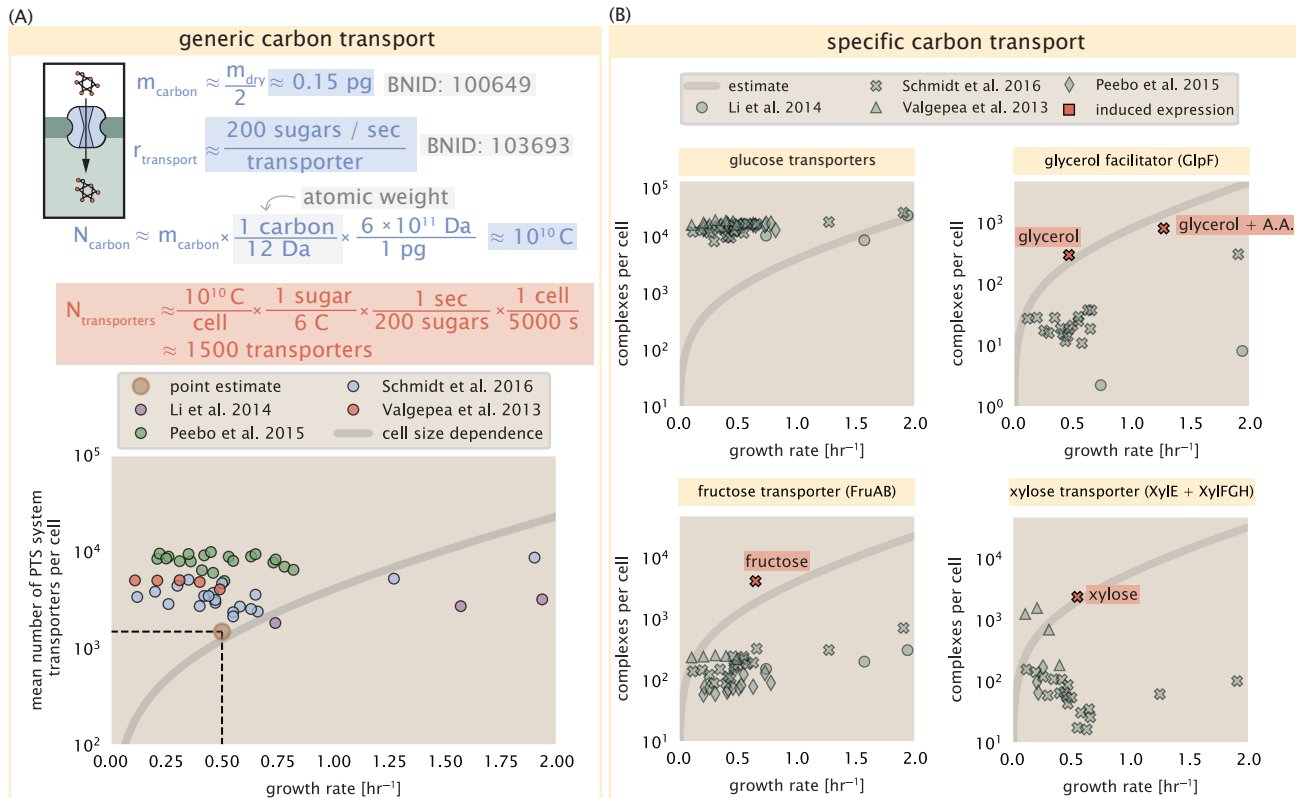


Figure 2. The abundance of carbon transport systems across growth rates. (A) A simple estimate for the minimum number of generic carbohydrate transport systems (top) assumes $\approx 10^{10}$ C are needed to complete division, each transported sugar contains ≈ 6 C, and each transporter conducts sugar molecules at a rate of ≈ 200 per second. Bottom plot shows the estimated number of transporters needed at a growth rate of ≈ 0.5 per hr (light-brown point and dashed lines). Colored points correspond to the mean number of PTS system sugar transporters (complexes annotated with the Gene Ontology term GO:0009401) for different growth conditions across different published datasets. (B) The abundance of various specific carbon transport systems plotted as a function of the population growth rate. The rates of substrate transport to compute the continuum growth rate estimate (grey line) were 200 glucose- s^{-1} (BNID: 103693, *Milo et al. (2010)*), 2000 glycerol- s^{-1} (*Lu et al., 2003*), 200 fructose- s^{-1} (assumed to be similar to PtsL, BNID: 103693, *Milo et al. (2010)*), and 50 xylose- s^{-1} (assumed to be comparable to LacY, BNID: 103159, *Milo et al. (2010)*). Red points and highlighted text indicate conditions in which the only source of carbon in the growth medium induces expression of the transport system. Grey line in (A) and (B) represents the estimated number of transporters per cell at a continuum of growth rates.

167 estimated number of transporters needed at each growth rate to satisfy the cellular carbon re-
 168 quirement. It is notable that in all cases, the magnitude of induced expression (shown in red) falls
 169 close to the estimate, illustrating the ability of the cell to tune expression in response to changing
 170 environments. Together, this generic estimation and the specific examples of induced expression
 171 suggest that transport of carbon across the cell membrane, while critical for growth, is not the
 172 rate-limiting step of cell division.

173 **Phosphorus and Sulfur Transport**

174 We now turn our attention towards other essential elements, namely phosphorus and sulfur. Phos-
 175 phorus is critical to the cellular energy economy in the form of high-energy phosphodiester bonds
 176 making up DNA, RNA, and the NTP energy pool as well as playing a critical role in the post-translational
 177 modification of proteins and defining the polar-heads of lipids. In total, phosphorus makes up
 178 $\approx 3\%$ of the cellular dry mass which in typical experimental conditions is in the form of inorganic
 179 phosphate. The cell membrane has remarkably low permeability to this highly-charged and critical
 180 molecule, therefore requiring the expression of active transport systems. In *E. coli*, the proton elec-
 181 trochemical gradient across the inner membrane is leveraged to transport inorganic phosphate
 182 into the cell (Rosenberg *et al.*, 1977). Proton-solute symporters are widespread in *E. coli* (Ramos
 183 and Kaback, 1977; Booth *et al.*, 1979) and can have rapid transport rates of 50 to 100 molecules
 184 per second for sugars and other solutes (BNID: 103159; 111777, Milo *et al.* (2010)). As a more
 185 extreme example, the proton transporters in the F₁-F₀ ATP synthase, which leverage the proton
 186 electrochemical gradient for rotational motion, can shuttle protons across the membrane at a rate
 187 of ≈ 1000 per second (BNID: 104890; 103390, (Milo *et al.*, 2010)). In *E. coli* the PitA phosphate trans-
 188 port system has been shown to be very tightly coupled with the proton electrochemical gradient
 189 with a 1:1 proton:phosphate stoichiometric ratio (Harris *et al.*, 2001; Feist *et al.*, 2007). Taking the
 190 geometric mean of the aforementioned estimates gives a plausible rate of phosphate transport
 191 on the order of 300 per second. Illustrated in *Figure 3(A)*, we can estimate that ≈ 150 phosphate
 192 transporters are necessary to maintain an $\approx 3\%$ dry mass with a 5000 s division time. This estimate
 193 is again satisfied when we examine the observed copy numbers of PitA in proteomic data sets (plot
 194 in *Figure 3(A)*). While our estimate is very much in line with the observed numbers, we emphasize
 195 that this is likely a slight overestimate of the number of transporters needed as there are other
 196 phosphorous scavenging systems, such as the ATP-dependent phosphate transporter Pst system
 197 which we have neglected.

198 Satisfied that there are a sufficient number of phosphate transporters present in the cell, we
 199 now turn to sulfur transport as another potentially rate limiting process. Similar to phosphate,
 200 sulfate is highly-charged and not particularly membrane permeable, requiring active transport.
 201 While there exists a H+/sulfate symporter in *E. coli*, it is in relatively low abundance and is not well
 202 characterized (Zhang *et al.*, 2014a). Sulfate is predominantly acquired via the ATP-dependent ABC
 203 transporter CysUWA system which also plays an important role in selenium transport (Sekowska
 204 *et al.*, 2000; Sirko *et al.*, 1995). While specific kinetic details of this transport system are not readily
 205 available, generic ATP transport systems in prokaryotes transport on the order of 1 to 10 molecules
 206 per second (BNID: 109035, Milo *et al.* (2010)). Combining this generic transport rate, measurement
 207 of sulfur comprising 1% of dry mass, and a 5000 second division time yields an estimate of ≈ 1000
 208 CysUWA complexes per cell (*Figure 3(B)*). Once again, this estimate is in notable agreement with
 209 proteomic data sets, suggesting that there are sufficient transporters present to acquire the nec-
 210 essary sulfur. In a similar spirit of our estimate of phosphorus transport, we emphasize that this is
 211 likely an overestimate of the number of necessary transporters as we have neglected other sulfur
 212 scavenging systems that are in lower abundance.

213 **Limits on Transporter Expression**

214 So which, if any, of these processes may be rate limiting for growth? As suggested by *Figure 2*
 215 (B), induced expression can lead to an order-of-magnitude (or more) increase in the amount of

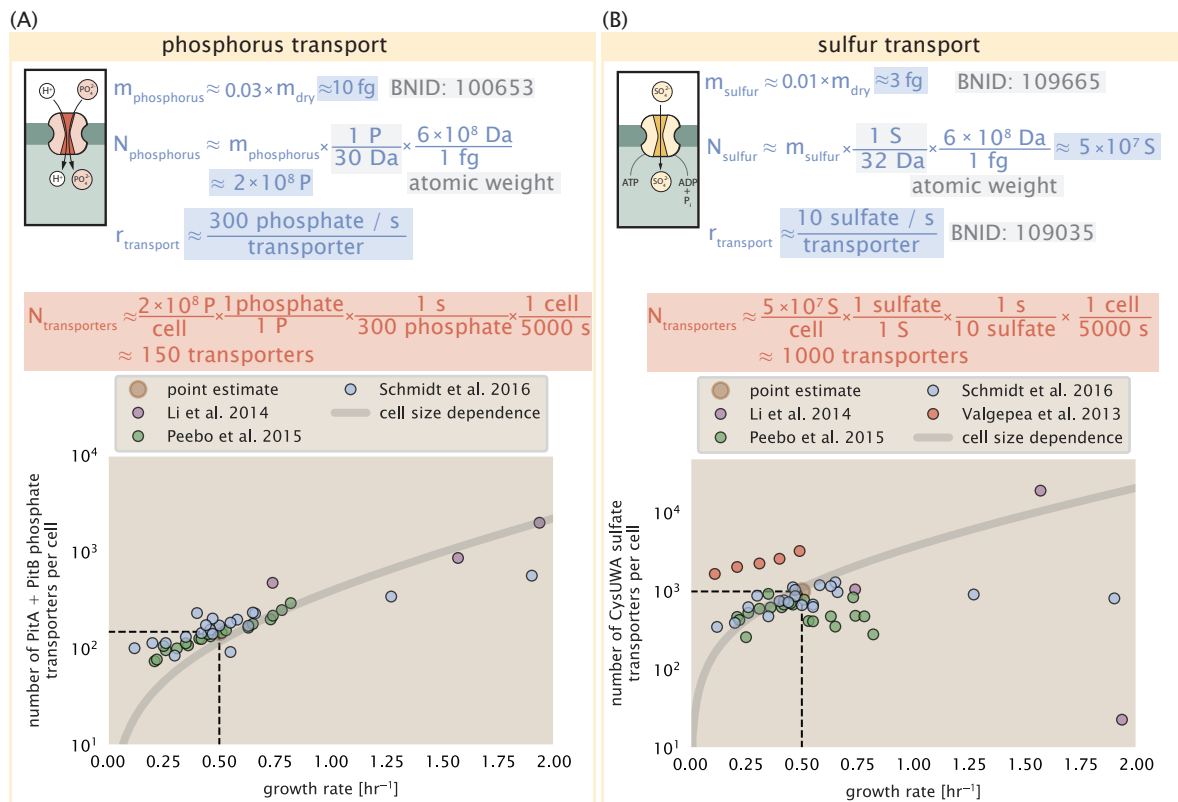


Figure 3. Estimates and measurements of phosphate and sulfate transport systems as a function of growth rate. (A) Estimate for the number of PitA phosphate transport systems needed to maintain a 3% phosphorus *E. coli* dry mass. Points in plot correspond to the total number of PitA transporters per cell. (B) Estimate of the number of CysUWA complexes necessary to maintain a 1% sulfur *E. coli* dry mass. Points in plot correspond to average number of CysUWA transporter complexes that can be formed given the transporter stoichiometry [CysA]₂[CysU][CysW][Sbp/CysP]. Grey line in (A) and (B) represents the estimated number of transporters per cell at a continuum of growth rates.

216 transporters needed to facilitate transport. Thus, if acquisition of nutrients was the limiting state
 217 in cell division, could expression simply be increased to accommodate faster growth? A way to
 218 approach this question is to compute the amount of space in the bacterial membrane that could
 219 be occupied by nutrient transporters. Considering a rule-of-thumb for the surface area of *E. coli* of
 220 about $6 \mu\text{m}^2$ (BNID: 101792, *Milo et al. (2010)*), we expect an areal density for 1000 transporters to
 221 be approximately 200 transporters/ μm^2 . For a typical transporter occupying about $50 \text{ nm}^2/\text{dimer}$,
 222 this amounts to about only 1 percent of the total inner membrane (*Szenk et al., 2017*). In addition,
 223 bacterial cell membranes typically have densities of 10^5 proteins/ μm^2 (*Phillips, 2018*), implying that
 224 the cell could accommodate more transporters of a variety of species if it were rate limiting. As we
 225 will see in the next section, however, occupancy of the membrane can impose other limits on the
 226 rate of energy production.

227 Energy Production

228 While the transport of nutrients is required to build new cell mass, the metabolic pathways both
 229 consume and generate energy in the form of NTPs. The high-energy phosphodiester bonds of
 230 (primarily) ATP power a variety of cellular processes that drive biological systems away from ther-
 231 modynamic equilibrium. The next set of processes we hypothesize might control the rate of cell
 232 division considers the energy budget of a dividing cell in terms of the synthesis of ATP from ADP
 233 and inorganic phosphate as well as maintenance of the electrochemical proton gradient which
 234 powers it.

235 ATP Synthesis

236 Hydrolysis of the terminal phosphodiester bond of ATP forming ADP and an inorganic phosphate is
 237 a kinetic driving force in a wide array of biochemical reactions. One such reaction is the formation
 238 of peptide bonds during translation which requires ≈ 2 ATPs for the charging of an amino acid
 239 to the tRNA and ≈ 2 ATP equivalents for the formation of the peptide bond between amino acids.
 240 Considering the ATP costs associated with error correction and post-translational modifications
 241 of proteins, we can make the approximation that each peptide bond has a net cost of ≈ 5 ATP
 242 (BNID: 107782, *Milo et al. (2010)*). In total, the energetic costs of peptide bond formation consume
 243 $\approx 80\%$ of the cells ATP budget (BNID: 107782; 106158; 101637; 111918, *Milo et al. (2010); Lynch*
and Marinov (2015); Stouthamer (1973)). The pool of ATP is produced by the F₁-F₀ ATP synthase
 245 – a membrane-bound rotary motor which under ideal conditions can yield ≈ 300 ATP per second
 246 (BNID: 114701; *Milo et al. (2010); Weber and Senior (2003)*).

247 To estimate the total number of ATP equivalents consumed during a cell cycle, we will make
 248 the approximation that there are $\approx 3 \times 10^6$ proteins per cell with an average protein length of ≈ 300
 249 peptide bonds (BNID: 115702; 108986; 104877, *Milo et al. (2010)*). Taking these values together,
 250 we estimate that the typical *E. coli* cell consumes $\approx 5 \times 10^9$ ATP per cell cycle on protein synthesis
 251 alone and $\approx 6 \times 10^9$ ATP in total. Assuming that the ATP synthases are operating at their fastest
 252 possible rate, ≈ 3000 ATP synthases are needed to keep up with the energy demands of the cell.
 253 This estimate and a comparison with the data are shown in *Figure 4* (A). Despite our assumption
 254 of maximal ATP production rate per synthase and approximation of all NTP consuming reactions
 255 being the same as ATP, we find that an estimate of a few thousand complete synthases per cell
 256 to agree well with the experimental data. Much as we did for the estimates of transporter copy
 257 number in the previous section, we can generalize this estimation to consider a continuum of
 258 growth rates rather than a point estimate of 5000 s, indicated by the gray lines in *Figure 4*, and find
 259 that this approach adequately describes the observed growth rate dependence.

260 If the direct production of ATP was a rate limiting step for growth, could the cell simply express
 261 more ATP synthase complexes? This requires us to consider several features of cellular physiology,
 262 namely the physical space on the inner membrane as well as the ability to maintain the proton
 263 chemical gradient leveraged by the synthase to drive ATP production out of equilibrium.

264 Generating the Proton Electrochemical Gradient

265 In order to produce ATP, the F₁-F₀ ATP synthase itself must consume energy. Rather than burning
 266 through its own product, this intricate macromolecular machine has evolved to exploit the elec-
 267 trochemical potential established across the inner membrane through cellular respiration. This
 268 electrochemical gradient is manifest by the pumping of protons into the intermembrane space via
 269 the electron transport chains as they reduce NADH. In *E. coli*, this potential difference is ≈ -200 mV
 270 (BNID: 102120, *Milo et al. (2010)*). A simple estimate of the inner membrane as a capacitor with a
 271 working voltage of -200 mV (as performed in the Supplemental Information) reveals that $\approx 2 \times 10^4$
 272 protons must be present in the intermembrane space.

273 However, the constant rotation of the ATP synthases would rapidly abolish this potential dif-
 274 ference if it were not being actively maintained. To undergo a complete rotation (and produce a
 275 single ATP), the F₁-F₀ ATP synthase must shuttle ≈ 4 protons across the membrane into the cytosol
 276 (BNID: 103390, *Milo et al. (2010)*). With ≈ 3000 ATP synthases each generating 300 ATP per second,
 277 the 2×10^4 protons establishing the 200 mV potential would be consumed in only a few millisec-
 278 onds. This brings us to our next estimate: how many electron transport complexes are needed to
 279 support the consumption rate of the ATP synthases?

280 The electrochemistry of the electron transport complexes of *E. coli* have been the subject of
 281 intense biochemical and biophysical study over the past half century (*Ingledew and Poole, 1984;*
282 Khademian and Imlay, 2017; Cox et al., 1970; Henkel et al., 2014). A recent work (*Szenk et al.,*
283 2017) examined the respiratory capacity of the *E. coli* electron transport complexes using struc-
 284 tural and biochemical data, revealing that each electron transport chain rapidly pumps protons
 285 into the intermembrane space at a clip of ≈ 1500 protons per second (BIND: 114704; 114687, *Milo*
286 et al. (2010)). Using our estimate of the number of ATP synthases required per cell (*Figure 4(A)*),
 287 coupled with these recent measurements, we estimate that ≈ 1000 electron transport complexes
 288 would be necessary to facilitate the $\approx 4 \times 10^6$ protons per second diet of the cellular ATP synthases.
 289 This estimate (along with a generalization to the entire range of observed growth rates) is in agree-
 290 ment with the number of complexes identified in the proteomic datasets (plot in *Figure 4(B)*). This
 291 suggests that every ATP synthase must be accompanied by ≈ 1 functional electron transport chain.
 292 Again, if this were a rate limiting process for bacterial growth, one must conclude that it is not
 293 possible for the cell to simply increase the production of both the number of electron transport
 294 chain complexes as well as ATP synthases. As both of these components only function bound to
 295 the inner membrane, we now turn our attention towards the available space in the membrane as
 296 well as surface-area-to-volume constraints.

297 Energy Production in a Crowded Membrane.

298 For each protein considered so far, the data shows that in general their numbers increase with
 299 growth rate. This is in part a consequence of the increase in cell length and width at that is common
 300 to many rod-shaped bacteria at faster growth rates (*Ojikic et al., 2019; Harris and Theriot, 2018*).
 301 For the particular case of *E. coli*, the total cellular protein and cell size increase logarithmically
 302 with growth rate (*Schaechter et al., 1958; Si et al., 2017*). Indeed, this is one reason why we have
 303 considered only a single, common growth condition across all our estimates so far. Such a scaling
 304 will require that the total number of proteins and net demand on resources also grow in proportion
 305 to the increase in cell size divided by the cell's doubling time. Recall however that each transport
 306 process, as well as the ATP production via respiration, is performed at the bacterial membrane.
 307 This means that their maximum productivity can only increase in proportion to the cell's surface
 308 area divided by the cell doubling time. This difference in scaling would vary in proportion to the
 309 surface area-to-volume (S/V) ratio.

310 While we found that there was more than sufficient membrane real estate for carbon intake in
 311 our earlier estimate, the total number of ATP synthases and electron chain transport complexes
 312 both exhibit a clear increase in copy number with growth rate, reaching in excess of 10^4 copies per
 313 cell (*Figure 4*). Here we consider the consequences of this S/V ratio scaling in more detail.

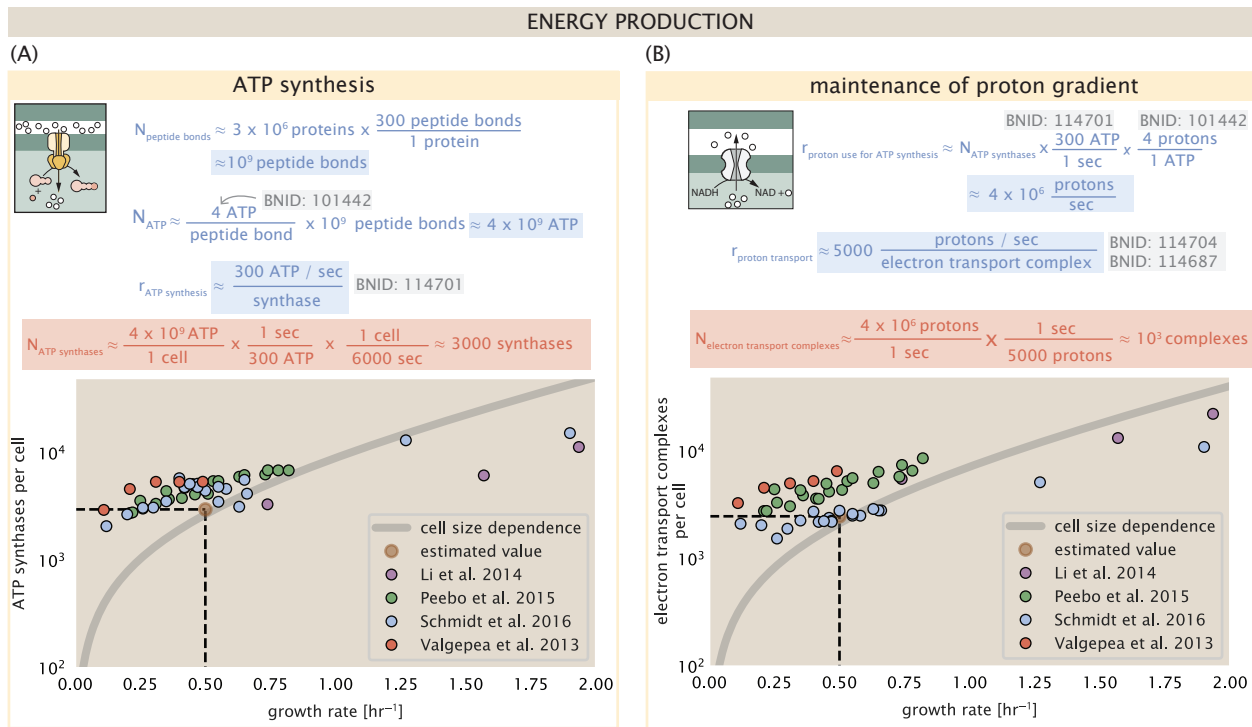


Figure 4. The abundance of F₁-F₀ ATP synthases and electron transport chain complexes as a function of growth rate. (A) Estimate of the number of F₁-F₀ ATP synthase complexes needed to accommodate peptide bond formation and other NTP dependent processes. Points in plot correspond to the mean number of complete F₁-F₀ ATP synthase complexes that can be formed given proteomic measurements and the subunit stoichiometry [AtpE]₁₀[AtpF]₂[AtpB][AtpC][AtpH][AtpA]₃[AtpG][AtpD]₃. (B) Estimate of the number of electron transport chain complexes needed to maintain a membrane potential of -200 mV given estimate of number of F₁-F₀ ATP synthases from (A). Points in plot correspond to the average number of complexes identified as being involved in aerobic respiration by the Gene Ontology identifier GO:0019646 that could be formed given proteomic observations. These complexes include cytochromes *bd*₁ ([CydA][CydB][CydX][CydH]), *bdII* ([AppC][AppB]), *bo₃*,([CyoD][CyoA][CyoB][CyoC]) and NADH:quinone oxioreductase I ([NuoA][NuoH][NuoJ][NuoK][NuoL][NuoM][NuoN][NuoB][NuoC][NuoE][NuoF][NuoG][NuoI]) and II ([Ndh]). Grey lines in both (A) and (B) correspond to the estimate procedure described, but applied to a continuum of growth rates. We direct the reader to the Supporting Information for a more thorough description of this approach.

314 In our estimate of ATP production above we found that a cell demands about 6×10^9 ATP or 10^6
 315 ATP/s. With a cell volume of roughly 1 fL, this corresponds to about 2×10^{10} ATP per fL of cell volume,
 316 in line with previous estimates (*Stouthamer and Bettenhausen, 1977; Szenk et al., 2017*). In **Figure 5**(A) we plot this ATP demand as a function of the S/V ratio in green, where we have considered
 317 a range of cell shapes from spherical to rod-shaped with an aspect ratio (length/width) equal to 4
 318 (See appendix for calculations of cell volume and surface area). In order to consider the maximum
 319 power that could be produced, we consider the amount of ATP that can be generated by a membrane
 320 filled with ATP synthase and electron transport complexes, which provides a maximal production
 321 of about 3 ATP / (nm²·s) (*Szenk et al., 2017*). This is shown in blue in **Figure 5**(A), which shows that
 322 at least for the growth rates observed, the energy demand is roughly an order of magnitude less.
 323

324 Interestingly, *Szenk et al. (2017)* also found that ATP production by respiration is less efficient
 325 than by fermentation per membrane area occupied due to the additional proteins of the electron
 326 transport chain. This suggests that even under anaerobic growth, there will be sufficient mem-
 327 brane space for ATP production in general.

328 While this serves to highlight the diminishing capacity to provide resources to grow if the cell
 329 increases in size (and its S/V decreases), the blue region in **Figure 5**(A) represents a somewhat
 330 unachievable limit since the inner membrane must also include other proteins such as those re-
 331 quired for lipid and membrane synthesis. To gain insight, we used the proteomic data to look at
 332 the distribution of proteins on the inner membrane. Here we use Gene Ontology (GO) annotations
 333 (*Ashburner et al., 2000; The Gene Ontology Consortium, 2018*) to identify all proteins embedded
 334 or peripheral to the inner membrane (GO term: 0005886). Those associated but not membrane-
 335 bound include proteins like MreB and FtsZ, that traverse the inner membrane by treadmilling and
 336 must nonetheless be considered as a vital component occupying space on the membrane. In **Fig-**
 337 **ure 5**(B), we find that the total protein mass per μm^2 is relatively constant with growth rate. Inter-
 338 estingly, when we consider the distribution of proteins grouped by their Clusters of Orthologous
 339 Groups (COG) (*Tatusov et al., 2000*), the relative abundance for those in metabolism (including ATP
 340 synthesis via respiration) is also relatively constant.

341 Function of the Central Dogma

342 Up to this point, we have considered a variety of transport and biosynthetic processes that are
 343 critical to acquiring and generating new cell mass. While there are of course many other metabolic
 344 processes we could consider and perform estimates of (such as the components of fermentative
 345 versus aerobic respiration), we now turn our focus to some of the most central processes which
 346 *must* be undertaken irrespective of the growth conditions – the processes of the central dogma.

347 DNA

348 Most bacteria (including *E. coli*) harbor a single, circular chromosome and can have extra-chromosomal
 349 plasmids up to ~ 100 kbp in length. We will focus our quantitative thinking solely on the chromo-
 350 some of *E. coli* which harbors ≈ 5000 genes and $\approx 5 \times 10^6$ base pairs. To successfully divide and
 351 produce viable progeny, this chromosome must be faithfully replicated and segregated into each
 352 nascent cell. We again rely on the near century of literature in molecular biology to provide some
 353 insight on the rates and mechanics of the replicative feat as well as the production of the required
 354 starting materials, dNTPs.

355 dNTP synthesis

356 We begin our exploration of DNA replication by examining the production of the deoxyribonucleotide
 357 triphosphates (dNTPs). The four major dNTPs (dATP, dTTP, dCTP, and dGTP) are synthesized *de*
 358 *novo* in separate pathways, requiring different building blocks. However, a critical step present in
 359 all dNTP synthesis pathways is the conversion from ribonucleotide to deoxyribonucleotide via the
 360 removal of the 3' hydroxyl group of the ribose ring (*Rudd et al., 2016*). This reaction is mediated
 361 by a class of enzymes termed ribonucleotide reductases, of which *E. coli* possesses two aerobically

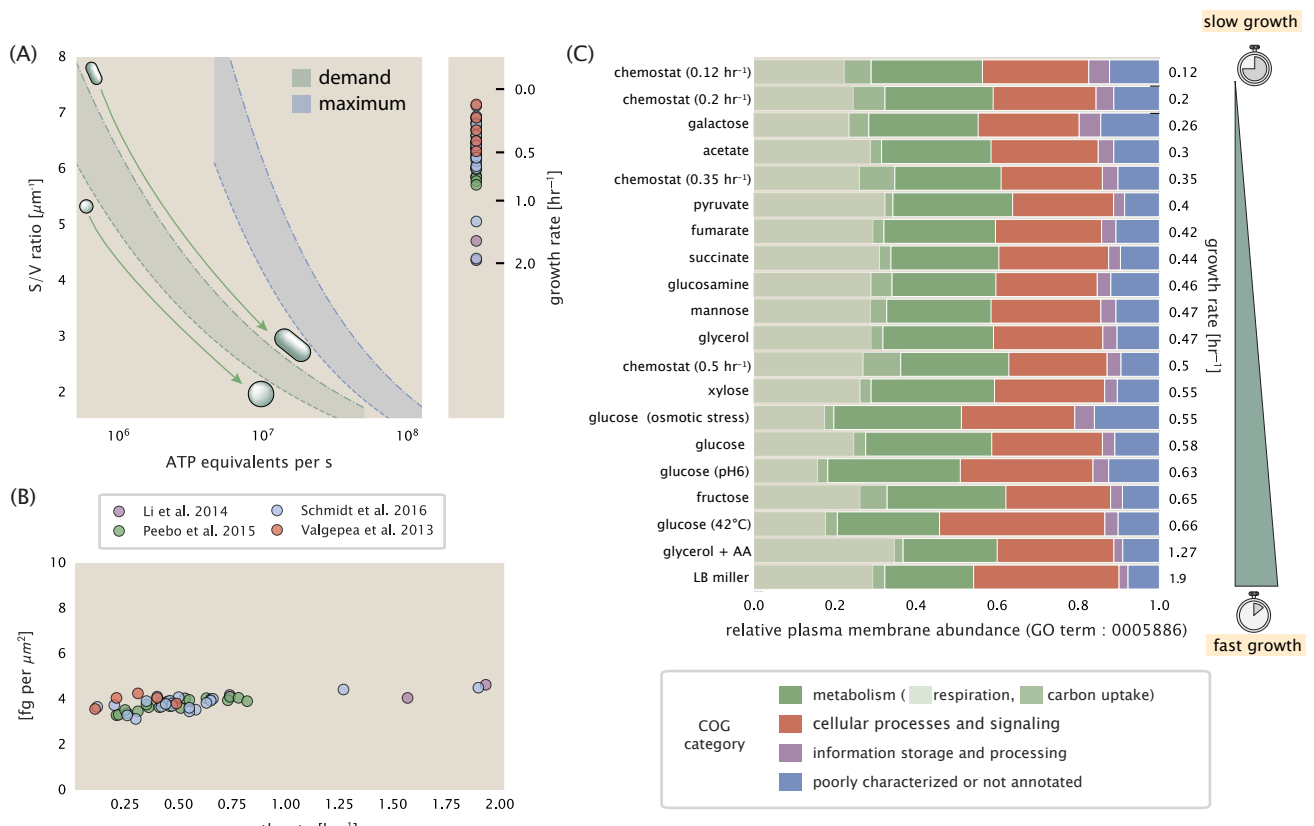


Figure 5. Influence of cell size and S/V ratio on ATP production and inner membrane composition. (A) Scaling of ATP demand and maximum ATP production as a function of S/V ratio. Cell volumes of 0.5 fL to 50 fL were considered, with the dashed (—) line corresponding to a sphere and the dash-dot line (---) reflecting a rod-shaped bacterium like *E. coli* with a typical aspect ratio (length / width) of 0.4 (Shi et al., 2018). Approximately 50% of the bacterial inner membrane is assumed to be protein, with the remainder lipid. (B) Total protein mass calculated for proteins with inner membrane annotation (GO term: 0005886). (C) Relative protein abundances by mass based on COG annotation. Metabolic proteins are further separated into respiration (F_1 - F_0 ATP synthase, NADH dehydrogenase I, succinate:quinone oxidoreductase, cytochrome bo₃ ubiquinol oxidase, cytochrome bd-I ubiquinol oxidase) and carbohydrate transport (GO term: GO:0008643). Note that the elongation factor EF-Tu can also associate with the inner membrane, but was excluded in this analysis due to its high relative abundance (roughly identical to the total mass shown in part (B)).

362 active complexes (termed I and II) and a single anaerobically active enzyme. Due to their peculiar
 363 formation of a radical intermediate, these enzymes have received much biochemical, kinetic, and
 364 structural characterization. One such work (**Ge et al., 2003**) performed a detailed *in vitro* measure-
 365 ment of the steady-state kinetic rates of these complexes, revealing a turnover rate of ≈ 10 dNTP
 366 per second.

367 Since this reaction is central to the synthesis of all dNTPs, it is reasonable to consider the abun-
 368 dence of these complexes is a measure of the total dNTP production in *E. coli*. Illustrated schemati-
 369 cally in **Figure 6** (A), we consider the fact that to replicate the cell's genome, on the order of $\approx 10^7$
 370 dNTPs must be synthesized. Assuming a production rate of 10 per second per ribonucleotide
 371 reductase complex and a cell division time of 5000 seconds, we arrive at an estimate of ≈ 200
 372 complexes needed per cell. As shown in the bottom panel of **Figure 6** (A), this estimate agrees
 373 with the experimental measurements of these complexes abundances within $\approx 1/2$ an order of
 374 magnitude. Extension of this estimate across a continuum of growth rate, including the fact that
 375 multiple chromosomes can be replicated at a given time, is shown as a grey transparent line in
 376 **Figure 6** (A). Similarly to our point estimate, this refinement agrees well with the data, accurately
 377 describing both the magnitude of the complex abundance and the dependence on growth rate.

378 Recent work has revealed that during replication, the ribonucleotide reductase complexes co-
 379 alesce to form discrete foci colocalized with the DNA replisome complex (**Sánchez-Romero et al.,**
 380 **2011**). This is particularly pronounced in conditions where growth is slow, indicating that spatial
 381 organization and regulation of the activity of the complexes plays an important role.

382 DNA Replication

383 We now turn our focus to the integration of these dNTP building blocks into the replicated chromo-
 384 some strand via the DNA polymerase. Replication is initiated at a single region of the chromosome
 385 termed the *oriC* locus at which a pair of DNA polymerases bind and begin their high-fidelity repli-
 386 cation of the genome in opposite directions. Assuming equivalence between the two replication
 387 forks, this means that the two DNA polymerase complexes (termed replisomes) meet at the mid-
 388 way point of the circular chromosome termed the *ter* locus. The kinetics of the five types of DNA
 389 polymerases (I – V) have been intensely studied, revealing that DNA polymerase III performs the
 390 high fidelity processive replication of the genome with the other "accessory" polymerases playing
 391 auxiliary roles (**Fijalkowska et al., 2012**). *In vitro* measurements have shown that DNA Polymerase
 392 III copies DNA at a rate of ≈ 600 nucleotides per second (BNID: 104120, **Milo et al. (2010)**). There-
 393 fore, to replicate a single chromosome, two replisomes (containing two DNA polymerase III each)
 394 moving at their maximal rate would copy the entire genome in ≈ 4000 s. Thus, with a division time
 395 of 5000 s (our "typical" growth rate for the purposes of this work), there is sufficient time for a pair
 396 of replisomes complexes to replicate the entire genome. However, this estimate implies that 4000
 397 s would be the upper-limit time scale for bacterial division which is at odds with the familiar 20
 398 minute (1200 s) doubling time of *E. coli* in rich medium.

399 It is well known that *E. coli* can parallelize its DNA replication such that multiple chromosomes
 400 are being replicated at once, with as many as 10 - 12 replication forks at a given time (**Bremer**
 401 **and Dennis, 2008; Si et al., 2017**). Thus, even in rapidly growing cultures, we expect only a few
 402 polymerases (≈ 10) are needed to replicate the chromosome per cell doubling. However, as shown
 403 in **Figure 6** (B), DNA polymerase III is nearly an order of magnitude more abundant. This
 404 discrepancy can be understood by considering its binding constant to DNA. DNA polymerase III is
 405 highly processive, facilitated by a strong affinity of the complex to the DNA. *In vitro* biochemical
 406 characterization has quantified the K_D of DNA polymerase III holoenzyme to single-stranded and
 407 double-stranded DNA to be 50 and 200 nM, respectively (**Ason et al., 2000**). The bottom plot in
 408 **Figure 6** (B) shows that the concentration of the DNA polymerase III across all data sets and growth
 409 conditions is within this range. Thus, while the copy number of the DNA polymerase III is in excess
 410 of the strict number required to replicate the genome, its copy number appears to vary such that its
 411 concentration is approximately equal to the dissociation constant to the DNA. While the processes

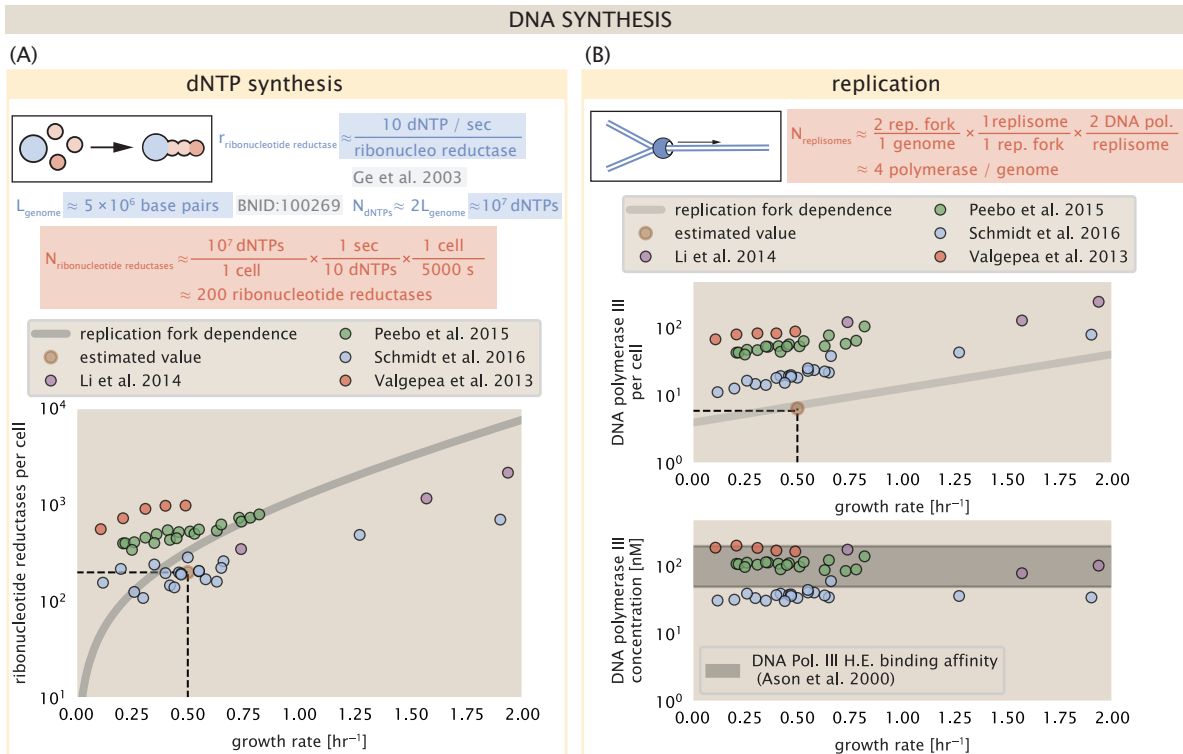


Figure 6. Complex abundance estimates for dNTP synthesis and DNA replication. (A) Estimate of the number of ribonucleotide reductase enzymes needed to facilitate the synthesis of $\approx 10^7$ dNTPs over the course of a 5000 second generation time. Points in the plot correspond to the total number of ribonucleotide reductase I ($[\text{NrdA}]_2[\text{NrdB}]_2$) and ribonucleotide reductase II ($[\text{NrdE}]_2[\text{NrdF}]_2$) complexes. (B) An estimate for the minimum number of DNA polymerase holoenzyme complexes needed to facilitate replication of a single genome. Points in the top plot correspond to the total number of DNA polymerase III holoenzyme complexes ($[\text{DnaE}]_3[\text{DnaQ}]_3[\text{HolE}]_3[\text{DnaX}]_5[\text{HolB}][\text{HolA}][\text{DnaN}]_4[\text{HolC}]_4[\text{HolD}]_4$) per cell. Bottom plot shows the effective concentration of DNA polymerase III holoenzyme given cell volumes calculated from the growth rate as in *Si et al. (2019)* (See Supplemental Information Section 4). Grey lines in (A) and top panel of (B) show the estimated number of complexes needed as a function of growth, the details of which are described in the Supplemental Information.

regulating the initiation of DNA replication are complex and involve more than just the holoenzyme, these data indicate that the kinetics of replication rather than the explicit copy number of the DNA polymerase III holoenzyme is the more relevant feature of DNA replication to consider. In light of this, the data in **Figure 6(B)** suggests that for bacteria like *E. coli*, DNA replication does not represent a rate-limiting step in cell division. However, it is worth noting that for bacterium like *C. crescentus* whose chromosomal replication is initiated only once per cell cycle (*Jensen et al., 2001*), the time to double their chromosome likely represents an upper limit to their growth rate.

RNA Synthesis

With the machinery governing the replication of the genome accounted for, we now turn our attention to the next stage of the central dogma – the transcription of DNA to form RNA. We primarily consider three major groupings of RNA, namely the RNA associated with ribosomes (rRNA), the RNA encoding the amino-acid sequence of proteins (mRNA), and the RNA which links codon sequence to amino-acid identity during translation (tRNA). Despite the varied function of these RNA species, they share a commonality in that they are transcribed from DNA via the action of RNA polymerase. In the coming paragraphs, we will consider the synthesis of RNA as a rate limiting step in bacterial division by estimating how many RNA polymerases must be present to synthesize all necessary rRNA, mRNA, and tRNA.

rRNA

We begin with an estimation of the number of RNA polymerases needed to synthesize the rRNA that serve as catalytic and structural elements of the ribosome. Each ribosome contains three rRNA molecules of lengths 120, 1542, and 2904 nucleotides (BNID: 108093, *Milo et al. (2010)*), meaning each ribosome contains ≈ 4500 nucleotides. As the *E. coli* RNA polymerase transcribes DNA to RNA at a rate of ≈ 40 nucleotides per second (BNID: 101904, *Milo et al. (2010)*), it takes a single RNA polymerase ≈ 100 s to synthesize the RNA needed to form a single functional ribosome. Therefore, in a 5000 s division time, a single RNA polymerase transcribing rRNA at a time would result in only ≈ 50 functional ribosomal rRNA units – far below the observed number of $\approx 10^4$ ribosomes per cell.

Of course, there can be more than one RNA polymerase transcribing the rRNA genes at any given time. To elucidate the *maximum* number of rRNA units that can be synthesized given a single copy of each rRNA gene, we will consider a hypothesis in which the rRNA operon is completely tiled with RNA polymerase. *In vivo* measurements of the kinetics of rRNA transcription have revealed that RNA polymerases are loaded onto the promoter of an rRNA gene at a rate of ≈ 1 per second (BNID: 111997; 102362, *Milo et al. (2010)*). If RNA polymerases are being constantly loaded on to the rRNA genes at this rate, then we can assume that ≈ 1 functional rRNA unit is synthesized per second. With a 5000 second division time, this hypothesis leads to a maximal value of 5000 functional rRNA units, still undershooting the observed number of 10^4 ribosomes per cell.

E. coli has evolved a clever mechanism to surpass this kinetic limit for the rate of rRNA production. Rather than having only one copy of each rRNA gene, *E. coli* has seven copies of the operon (BIND: 100352, *Milo et al. (2010)*) four of which are localized directly adjacent to the origin of replication (*Birnbaum and Kaplan, 1971*). As fast growth also implies an increased gene dosage due to parallelized chromosomal replication, the total number of rRNA genes can be on the order of $\approx 10 - 70$ copies at moderate to fast growth rates (*Stevenson and Schmidt, 2004*). Using our standard time scale of a 5000 second division time, we can make the lower-bound estimate that the typical cell will have 7 copies of the rRNA operon. Synthesizing one functional rRNA unit per second per rRNA operon, a total of 4×10^4 rRNA units can be synthesized, comfortably above the observed number of ribosomes per cell.

How many RNA polymerases are then needed to constantly transcribe 7 copies of the rRNA genes? We approach this estimate by considering the maximum number of RNA polymerases tiled along the rRNA genes with a loading rate of 1 per second and a transcription rate of 40 nucleotides per second. Considering that a RNA polymerase has a physical footprint of approximately 40 nu-

461 cleotides (BNID: 107873, *Milo et al. (2010)*), we can expect ≈ 1 RNA polymerase per 80 nucleotides.
462 With a total length of ≈ 4500 nucleotides per operon and 7 operons per cell, the maximum number
463 of RNA polymerases that can be transcribing rRNA at any given time is ≈ 400 . As we will see in the
464 coming sections, the synthesis of rRNA is the dominant requirement of the RNA polymerase pool.

465 mRNA

466 To form a functional protein, all protein coding genes must first be transcribed from DNA to form
467 an mRNA molecule. While each protein requires an mRNA blueprint, many copies of the protein
468 can be synthesized from a single mRNA. Factors such as strength of the ribosomal binding site,
469 mRNA stability, and rare codon usage frequency dictate the number of proteins that can be made
470 from a single mRNA, with yields ranging from 10^1 to 10^4 (BNID: 104186; 100196; 106254, *Milo et al.*
471 (2010)). Computing the geometric mean of this range yields ≈ 1000 proteins synthesized per mRNA,
472 a value that agrees with experimental measurements of the number of proteins per cell ($\approx 3 \times 10^6$,
473 BNID: 100088, *Milo et al. (2010)*) and total number of mRNA per cell ($\approx 3 \times 10^3$, BNID: 100064, *Milo*
474 *et al. (2010)*).

475 This estimation captures the *steady-state* mRNA copy number, meaning that at any given time,
476 there will exist approximately 3000 unique mRNA molecules. To determine the *total* number of
477 mRNA that need to be synthesized over the cell's lifetime, we must consider degradation of the
478 mRNA. In most bacteria, mRNAs are rather unstable with life times on the order of several minutes
479 (BNID: 104324; 106253; 111927; 111998, *Milo et al. (2010)*). For convenience, we assume that the
480 typical mRNA in our cell of interest has a typical lifetime of ≈ 300 seconds. Using this value, we
481 can determine the total mRNA production rate to maintain a steady-state copy number of 3000
482 mRNA per cell. While we direct the reader to the appendix for a more detailed discussion of mRNA
483 transcriptional dynamics, we state here that the total mRNA production rate must be on the order
484 of ≈ 15 mRNA per second. In *E. coli*, the average protein is ≈ 300 amino acids in length (BNID:
485 108986; *Milo et al. (2010)*), meaning that the corresponding mRNA is ≈ 900 nucleotides which we
486 will further approximate as ≈ 1000 nucleotides to account for the non-protein coding regions on
487 the 5' and 3' ends. This means that the cell must have enough RNA polymerase molecules about
488 to sustain a transcription rate of $\approx 1.5 \times 10^4$ nucleotides per second. Knowing that a single RNA
489 polymerase polymerizes RNA at a clip of 40 nucleotides per second, we arrive at a comfortable
490 estimate of ≈ 250 RNA polymerase complexes needed to satisfy the mRNA demands of the cell. It
491 is worth noting that this number is approximately half of that required to synthesize enough rRNA,
492 as we saw in the previous section. We find this to be a striking result as these 250 RNA polymerase
493 molecules are responsible for the transcription of the ≈ 4000 protein coding genes that are not
494 ribosome associated.

495 tRNA

496 The final class of RNA molecules worthy of quantitative consideration is the the pool of tRNAs
497 used during translation to map codon sequence to amino acid identity. Unlike mRNA or rRNA,
498 each individual tRNA is remarkably short, ranging from 70 to 95 nucleotides each (BNID: 109645;
499 102340, *Milo et al. (2010)*). What they lack in length, they make up for in abundance. There are
500 many measurements of the size of the *E. coli* tRNA pool, ranging from $\approx 6 \times 10^4$ (BNID: 105280, *Milo*
501 *et al. (2010)*) to $\approx 4 \times 10^5$ (BNID: 108611). To test tRNA synthesis as a possible growth-rate limiting
502 stage, we will err towards a higher abundance of $\approx 4 \times 10^5$ per cell. Combining the abundance and
503 tRNA length measurements, we make the estimate that $\approx 5 \times 10^7$ nucleotides are sequestered in
504 tRNA per cell. Unlike mRNA, tRNA is remarkably stable with typical lifetimes *in vivo* on the order of
505 ≈ 48 hours (*Abelson et al., 1974; Svenningsen et al., 2017*) – well beyond the timescale of division.
506 Once again using our rule-of-thumb for the rate of transcription to be 40 nucleotides per second
507 and assuming a division time of ≈ 5000 seconds, we arrive at an estimate of ≈ 150 RNA polymerases
508 to synthesize enough tRNA. This requirement pales in comparison to the number of polymerases
509 needed to generate the rRNA and mRNA pools and can be neglected as a significant transcriptional

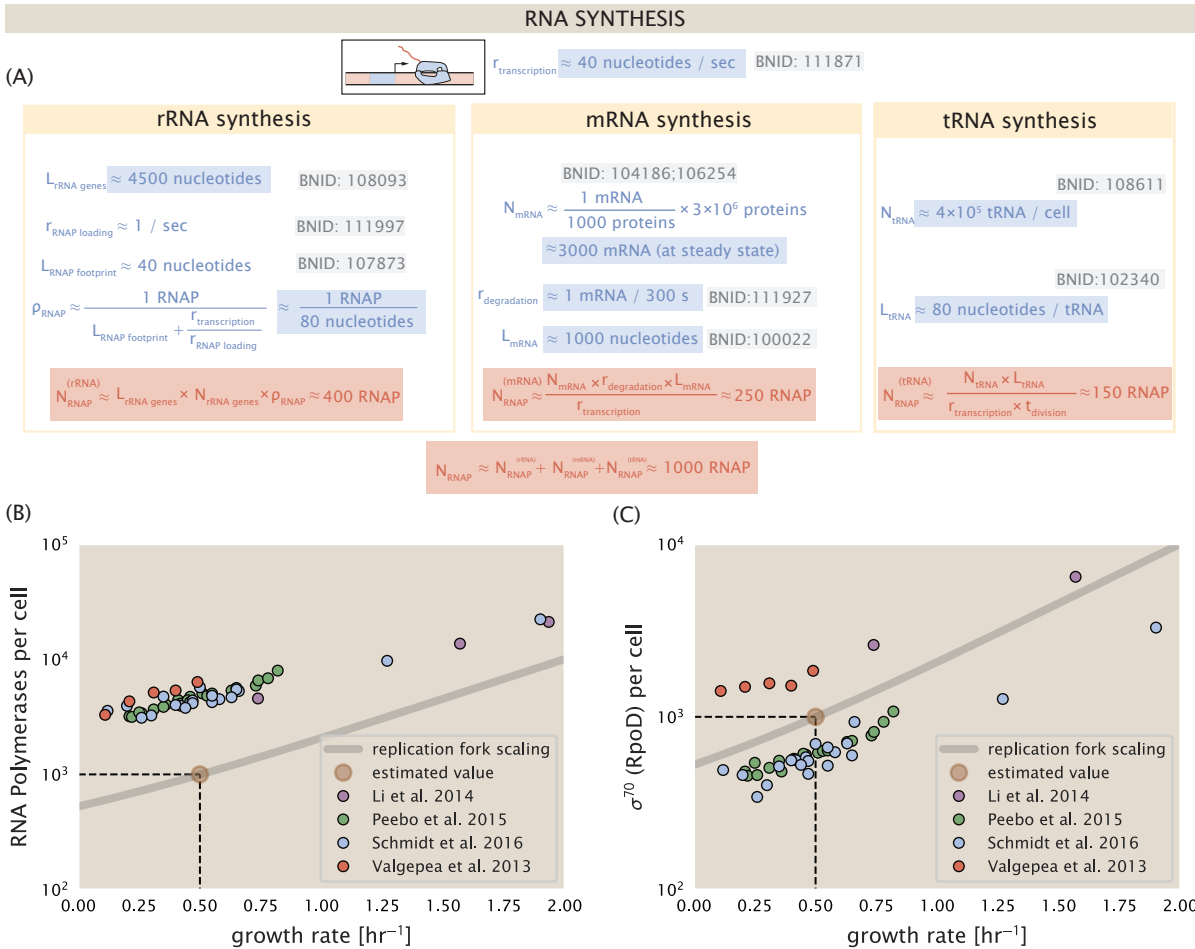


Figure 7. Estimation of the RNA polymerase demand and comparison with experimental data. (A)

Estimations for the number of RNA polymerase needed to synthesize sufficient quantities of rRNA, mRNA, and tRNA from left to right, respectively. Bionumber Identifiers (BNIDs) are provided for key quantities used in the estimates. (B) The RNA polymerase core enzyme copy number as a function of growth rate. Colored points correspond to the average number RNA polymerase core enzymes that could be formed given a subunit stoichiometry of $[RpoA]_2[RpoC][RpoB]$. (C) The abundance of σ^{70} as a function of growth rate. Estimated value for the number of RNAP is shown in (B) and (C) as a translucent brown point at a growth rate of 0.5 hr^{-1} .

510 burden.

511 RNA Polymerase and σ -factor Abundance

512 These estimates, summarized in **Figure 7 (A)**, reveal that synthesis of rRNA and mRNA are the domi-
513 nant RNA species synthesized by RNA polymerase, suggesting the need for ≈ 700 RNA polymerases
514 per cell. As is revealed in **Figure 7 (B)**, this estimate is about an order of magnitude below the ob-
515 served number of RNA polymerase complexes per cell ($\approx 5000 - 7000$). The disagreement between
516 the estimated number of RNA polymerases and these observations are at least consistent with
517 recent literature revealing that $\approx 80\%$ of RNA polymerases in *E. coli* are not transcriptionally active
518 (*Patrick et al., 2015*). Our estimate ignores the possibility that some fraction is only nonspecifically
519 bound to DNA, as well as the obstacles that RNA polymerase and DNA polymerase present for each
520 other as they move along the DNA (*Finkelstein and Greene, 2013*).

521 In addition, it is also vital to consider the role of σ -factors which help RNA polymerase identify
522 and bind to transcriptional start sites (*Browning and Busby, 2016*). Here we consider σ^{70} (RpoD)
523 which is the dominant "general-purpose" σ -factor in *E. coli*. While initially thought of as being solely

involved in transcriptional initiation, the past two decades of single-molecule work has revealed a more multipurpose role for σ^{70} including facilitating transcriptional elongation (*Kapanidis et al., 2005; Goldman et al., 2015; Perdue and Roberts, 2011; Mooney and Landick, 2003; Mooney et al., 2005*). **Figure 7** (B) is suggestive of such a role as the number of σ^{70} proteins per cell is in close agreement with our estimate of the number of transcriptional complexes needed.

These estimates provide insight as to the observed magnitude of both RNA polymerase and the σ -70 factor. As we have done in the previous sections, and described in the supplemental information, we can generalize these estimates across a wide range of growth rates (grey line in **Figure 7(B)**). While there remains some disagreement in the magnitude of the copy number, this estimate appears to very adequately describe the growth rate dependence of these complexes. Furthermore, these findings illustrate that transcription cannot be the rate limiting step in bacterial division. **Figure 7** (A) reveals that the availability of RNA polymerase is not a limiting factor for cell division as the cell always has an apparent \sim 10-fold excess than needed. Furthermore, if more transcriptional activity was needed to satisfy the cellular requirements, more σ^{70} -factors could be expressed to utilize a larger fraction of the RNA polymerase pool.

539 Translation and ribosomal synthesis

540 Lastly, we turn our attention to the process of synthesizing new proteins, translation. This process
 541 stands as a good candidate for potentially limiting growth since the synthesis of new proteins relies
 542 on the generation of ribosomes, themselves proteinaceous molecules. As we will see in the coming
 543 sections of this work, this poses a "chicken-or-the-egg" problem where the synthesis of ribosomes
 544 requires ribosomes in the first place.

545 We will begin our exploration of protein translation in the same spirit as we have in previous sections – we will draw order-of-magnitude estimates based on our intuition and available literature,
 546 and then compare these estimates to the observed data. In doing so, we will estimate both the
 547 absolute number of ribosomes necessary for replication of the proteome as well as the synthesis
 548 of amino-acyl tRNAs. From there we consider the limitations on ribosomal synthesis in light of our
 549 estimates on both, the synthesis of ribosomal proteins, and our earlier results on rRNA synthesis.

551 tRNA synthetases

552 We begin by first estimating the number of tRNA ligases in *E. coli* needed to convert free amino-
 553 acids to polypeptide chains. At a modest growth rate of \approx 5000 s, *E. coli* has roughly 3×10^6 proteins
 554 per cell (BNID: 115702; *Milo et al. (2010)*). Assuming that the typical protein is on the order of \approx
 555 300 amino acids in length (BNID: 100017; *Milo et al. (2010)*), we can estimate that a total of $\approx 10^9$
 556 amino acids are stitched together by peptide bonds.

557 How many tRNAs are needed to facilitate this remarkable number of amino acid delivery events
 558 to the translating ribosomes? It is important to note that tRNAs are recycled after they've passed
 559 through the ribosome and can be recharged with a new amino acid, ready for another round of
 560 peptide bond formation. While some *in vitro* data exists on the turnover of tRNA in *E. coli* for
 561 different amino acids, we can make a reasonable estimate by comparing the number of amino
 562 acids to be polymerized to cell division time. Using our stopwatch of 5000 s and 10^9 amino acids,
 563 we arrive at a requirement of $\approx 2 \times 10^5$ tRNA molecules. This estimate is in line with experimental
 564 measurements of $\approx 3 \times 10^5$ per cell (BNID: 108611, *Milo et al. (2010)*), suggesting we are on the
 565 right track.

566 There are many processes which go into synthesizing a tRNA and ligating it with the appropriate
 567 amino acids. As we covered in the previous section, there appear to be more than enough RNA
 568 polymerases per cell to synthesize the needed pool of tRNAs. Without considering the many ways
 569 in which amino acids can be scavenged or synthesized *de novo*, we can explore ligation the as a
 570 potential rate limiting step. The enzymes which link the correct amino acid to the tRNA, known as
 571 tRNA synthetases or tRNA ligases, are incredible in their proofreading of substrates with the incor-
 572 rect amino acid being ligated once out of every 10^4 to 10^5 times (BNID: 103469, *Milo et al. (2010)*).

573 This is due in part to the consumption of energy as well as a multi-step pathway to ligation. While
 574 the rate at which tRNA is ligated is highly dependent on the identity of the amino acid, it is reason-
 575 able to state that the typical tRNA synthetase has charging rate of ≈ 20 AA per tRNA synthetase per
 576 second (BNID: 105279, *Milo et al. (2010)*).

577 Combining these estimates together, as shown schematically in *Figure 8(A)*, yields an estimate
 578 of $\approx 10^4$ tRNA synthetases per cell with a division time of 5000 s. This point estimate is in very close
 579 agreement with the observed number of synthetases (the sum of all 20 tRNA synthetases in *E. coli*).
 580 This estimation strategy seems to adequately describe the observed growth rate dependence of
 581 the tRNA synthetase copy number (shown as the grey line in *Figure 8(B)*), suggesting that the copy
 582 number scales with the cell volume.

583 In total, the estimated and observed $\approx 10^4$ tRNA synthetases occupy only a meager fraction of
 584 the total cell proteome, around 0.5% by abundance. It is reasonable to assume that if tRNA charg-
 585 ing was a rate limiting process, cells would be able to increase their growth rate by devoting more
 586 cellular resources to making more tRNA synthases. As the synthesis of tRNAs and the correspond-
 587 ing charging can be highly parallelized, we can argue that tRNA charging is not a rate limiting step
 588 in cell division, at least for the growth conditions explored in this work.

589 Protein synthesis

590 With the number of tRNA synthetases accounted for, we now consider the abundance of the pro-
 591 tein synthesis machines themselves, ribosomes. Ribosomes are enormous protein/rRNA com-
 592 plexes that facilitate the peptide bond formation between amino acids in the correct sequence
 593 as defined by the coding mRNA. Before we examine the synthesis of the ribosome proteins and
 594 the limits that may place on the observed bacterial growth rates, let's consider replication of the
 595 cellular proteome.

596 As described in the previous section, *E. coli* consists of $\approx 3 \times 10^6$ proteins at a growth rate of \approx
 597 5000 s. If we again assume that each protein is composed of ≈ 300 amino acids and each amino
 598 acid is linked together by one peptide bond, we arrive at an estimate that the cellular proteome
 599 consists of $\approx 10^{10}$ peptide bonds. While the rate at which ribosomes translates is well known to
 600 have a growth rate dependence *Dai et al. (2018)* and is a topic which we discuss in detail in the
 601 coming sections. However, for the purposes of our order-of-magnitude estimate, we can make
 602 the approximation that translation occurs at a rate of ≈ 15 amino acids per second per ribosome
 603 (BNID: 100233, *Milo et al. (2010)*). Under this approximation and assuming a division time of 5000
 604 s, we can arrive at an estimate of $\approx 10^4$ ribosomes are needed to replicate the cellular proteome,
 605 shown in *Figure 8(B)*. This point estimate, while glossing over important details such as chromo-
 606 some copy number and growth-rate dependent translation rates, proves to be notably accurate
 607 when compared to the experimental observations (*Figure 8(B)*).

608 Translation as a growth-rate limiting step

609 Thus far, the general back-of-the-envelope estimates have been reasonably successful in explain-
 610 ing what sets the scale of absolute protein copy number. A recurring theme that has arisen is the
 611 ability of cells to parallelize their biosynthesis tasks. For example, while DNA replication speed-limit
 612 is ≈ 40 minutes to replicate a genome, cells can divide faster than this by initiating more than one
 613 round of replication per doubling. However, as we will see, parallelization is not possible when it
 614 comes to the translation of ribosomal proteins (*Figure 9(A)*). Thus, it is plausible that translation
 615 may be a key factor in determining the cellular growth rate.

616 To gain some intuition into how translation can set the speed of bacterial growth, we again
 617 consider the total number of peptide bonds that must be synthesized, which we denote as N_{AA} .
 618 Noting that cells grow exponentially in time (*Godin et al., 2010*), we can compute the number of
 619 amino acids to be polymerized as

$$N_{AA}\lambda = r_t R, \quad (1)$$

620 where λ is the cell growth rate in s^{-1} , r_t is the maximum translation rate in $AA \cdot s^{-1}$, and R is the

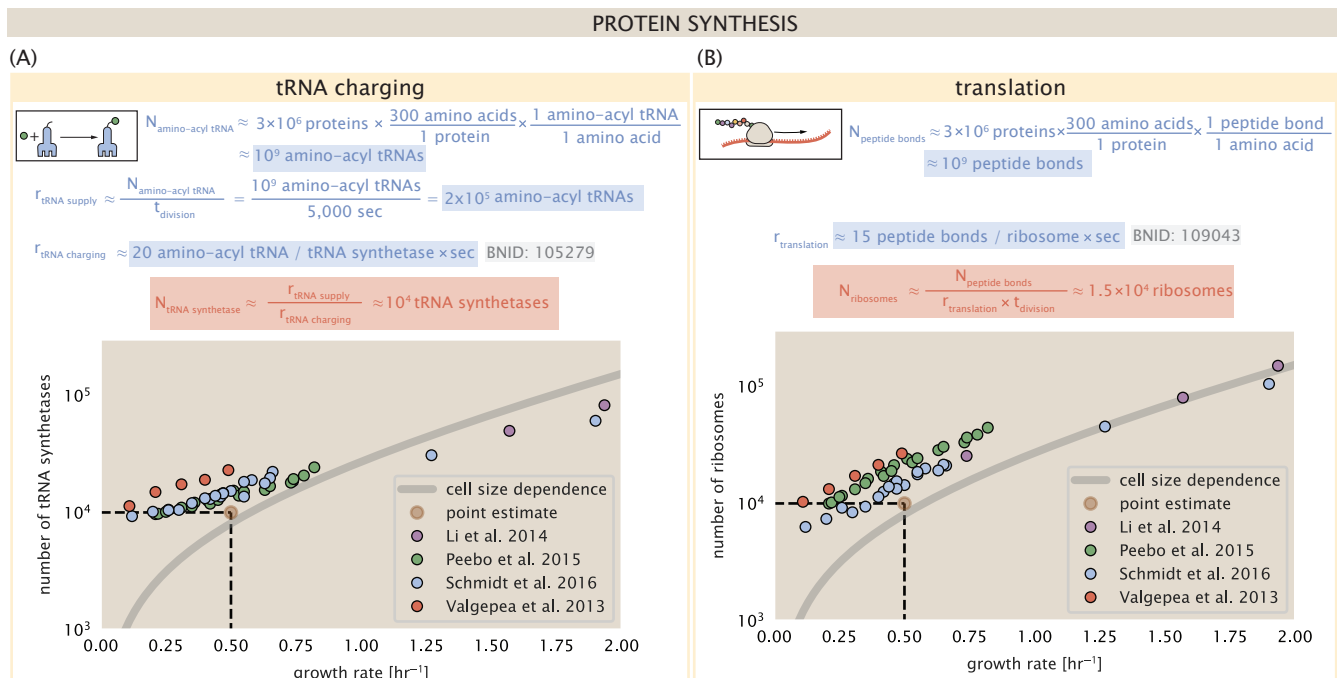


Figure 8. Estimation of the required tRNA synthetases and ribosomes. (A) Estimation for the number of tRNA synthetases that will supply the required amino acid demand. The sum of all tRNA synthetases copy numbers are plotted as a function of growth rate ([ArgS], [CysS], [GlnS], [Glx], [IleS], [LeuS], [ValS], [AlaS]₂, [AsnS]₂, [AspS]₂, [TyrS]₂, [TrpS]₂, [ThrS]₂, [SerS]₂, [ProS]₂, [PheS]₂[PheT]₂, [MetG]₂, [LysS]₂, [HisS]₂, [GlyS]₂[GlyQ]₂). (B) Estimation of the number of ribosomes required to synthesize 10⁹ peptide bonds with an elongation rate of 15 peptide bonds per second. The average abundance of ribosomes is plotted as a function of growth rate. Our estimated values are shown for a growth rate of 0.5 hr⁻¹. Grey lines correspond to the estimated complex abundance calculated at different growth rates. See Supplemental Information XX for a more detail description of this calculation.

621 average ribosome copy number per cell. Knowing the number of peptide bonds to be formed
 622 permits us to compute the translation-limited growth rate as

$$\lambda_{\text{translation-limited}} = \frac{r_t R}{N_{\text{AA}}} \quad (2)$$

623 Alternatively, since N_{AA} is related to the total protein mass through the molecular weight of
 624 each protein, we can also consider the growth rate in terms of the fraction of the total proteome
 625 mass that is dedicated to ribosomal protein mass. By making the approximation that an average
 626 amino acid has a molecular weight of 110 Da (BNID: 104877, *Milo et al. (2010)*), we can approximate
 627 $R/N_{\text{AA}} \approx \Phi_R/L_R$, where Φ_R is the ribosomal mass fraction and L_R is the total length in amino acids
 628 that make up a ribosome. The translation-limited growth rate can then be written in the form

$$\lambda_{\text{translation-limited}} \approx \frac{r_t}{L_R} \Phi_R \quad (3)$$

629 This is plotted as a function of ribosomal fraction Φ_R in **Figure 9(B)**, where we take $L_R \approx 7500$ AA,
 630 corresponding to the length in amino acids for all ribosomal subunits of the 50S and 30S complex
 631 (BNID: 101175, *(Milo et al., 2010)*).

632 The growth rate defined by **Equation 3** reflects mass-balance under steady-state growth and
 633 has long provided a rationalization of the apparent linear increase in *E. coli*'s ribosomal content
 634 as a function of growth rate (*Maaløe, 1979; Scott et al., 2010*). We note that there is a maximum
 635 growth rate of $\lambda \approx 8 \text{ hr}^{-1}$, or a doubling time just under 6 minutes (**Figure 9(B)**, dashed line). This
 636 represents an inherent speed limit due to the need for the cell to double its entire ribosomal mass.
 637 Interestingly, this limit is independent of the absolute number of ribosomes and is simply given by
 638 the time to translate an entire ribosome, L_R/r_t . As shown in **Figure 9(A)**, we can reconcile this with
 639 the observation that in order to double the average number of ribosomes, each ribosome must
 640 produce a second ribosome and cannot be parallelized.

641 Earlier, we considered rRNA synthesis (see Section **RNA Synthesis**), finding that, when the rRNA
 642 operons are maximally loaded with RNA polymerase, the cell can produce ≈ 1 functional rRNA unit
 643 per second per operon. In **Figure 9(C)**, we show the maximum number of ribosomes that could
 644 be made as a function of growth rate given this rRNA production rule-of-thumb. While each *E.*
 645 *coli* genome has 7 copies of the rRNA operon (BNID: 107866, *Milo et al. (2010)*), parallelization
 646 of DNA synthesis by firing multiple rounds of replication at a time can drastically the effective
 647 number of rRNA operons. The blue curve in ??, we assume that the effective number of rRNA
 648 operons increases in proportion to the number of origins of replication ($\# \text{ ori}$) (solid blue line;
 649 with the calculation of ($\# \text{ ori}$) described in the next section). Although we expect this value to
 650 drastically overestimate rRNA abundance at slower growth rates ($\lambda < 0.5 \text{ hr}^{-1}$), it provides a useful
 651 reference when considered along with the proteomic measurements that are also plotted. For
 652 growth rates above about 1 hr^{-1} , we find that cells will need to transcribe rRNA near their maximal
 653 rate. The dashed blue curve in **Figure 9(C)** shows the maximal number of functional rRNA units
 654 that could be synthesized from a single genome (ignoring the chromosome replication speed limit
 655 of ≈ 40 minutes per genome). The convergence between the maximum rRNA production with
 656 parallelization and the experimentally measured ribosome copy number (points in **Figure 9(C)**),
 657 as well as the observation cells are rarely reported to grow faster than 2 hr^{-1} [GC: Can we find a
 658 citation for this?], suggests rRNA synthesis represents the rate limiting step in cell division for this
 659 strain of *E. coli*.

660 Relationship between cell size and growth rate.

661 With the observation that ribosomes set an inherent upper limit on growth rate, through both rRNA
 662 synthesis and the additional dependence on ribosomal fraction, it is also plausible that ribosomes
 663 may play a more dominant role in setting growth rate across other growth conditions. With a rich
 664 proteomic data set across a wide array of conditions, and in light of a number of recent experi-
 665 mental observations, we find that cells also appear to tune their ribosomal abundance as a means

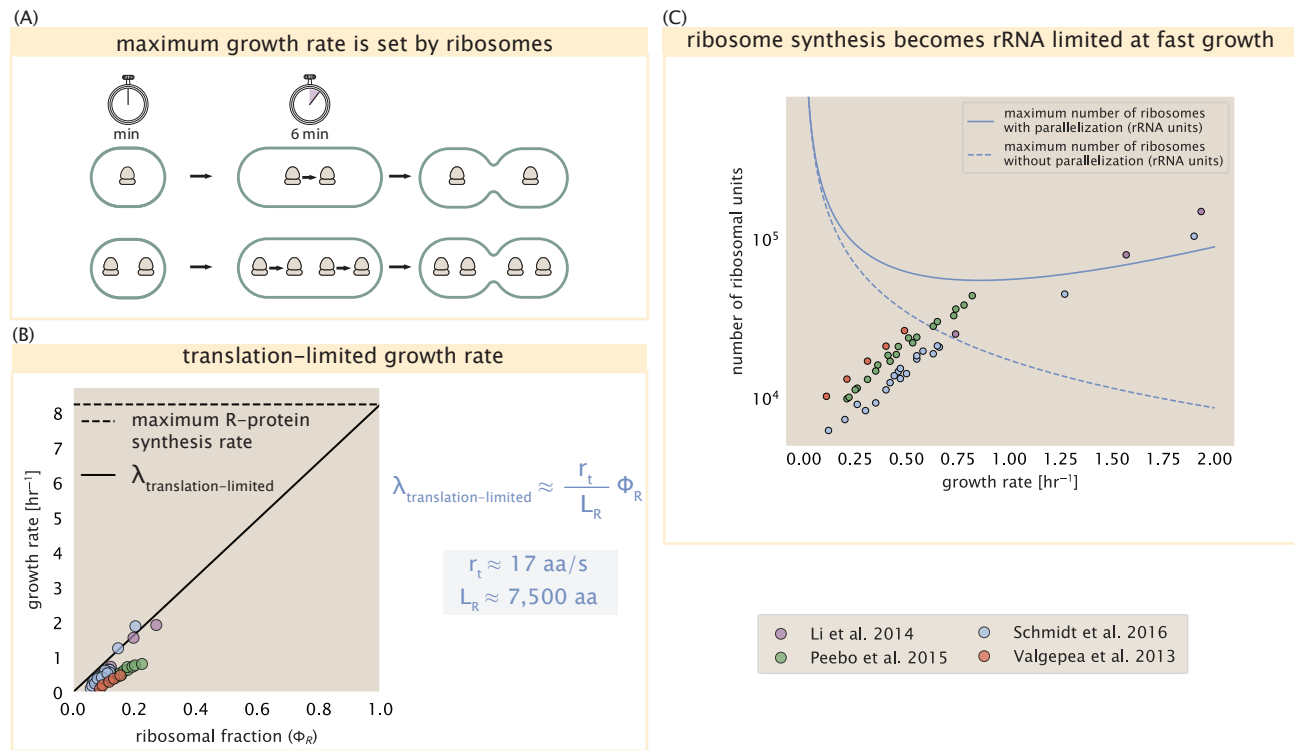


Figure 9. Translation-limited growth rate. (A) Here we consider the translation-limited growth rate as a function of ribosomal fraction. By mass balance, the time required to double the entire proteome (N_{AA} / r_t) sets the translation-limited growth rate, $\lambda_{\text{translation-limited}}$. Here N_{AA} is effectively the number of peptide bonds that must be translated, r_t is the translation elongation rate, and R is the number of ribosomes. This can also be re-written in terms of the ribosomal mass fraction $\Phi_R = m_R / m_{\text{protein}}$, where m_R is the total ribosomal mass and m_{protein} is the mass of all proteins in the cell. L_R refers to the summed length of the ribosome in amino acids. $\lambda_{\text{translation-limited}}$ is plotted as a function of Φ_R (solid line). (B) The dashed line in part (A) identifies a maximum growth rate that is set by the ribosome. Specifically, this growth rate corresponds to the time required to translate an entire ribosome, L_R / r_t . This is a result that is independent of the number of ribosomes in the cell as shown schematically here. (C) Maximum number of rRNA units that can be synthesized as a function of growth rate. Solid curve corresponds to the rRNA copy number calculated by multiplying the number of rRNA operons by the estimated number of (# ori) at each growth rate. The quantity (# ori) was calculated using Equation 4 and the measurements from Si et al. (2017) that are plotted in Figure 10(A). Dashed line show that maximal number of functional rRNA units produced from a single chromosome without parallelization.

666 to maximize growth even in poor nutrient conditions. This has important consequences on the
 667 relationship with cell size and maintenance of steady-state growth. In the coming section and the
 668 remainder of the text, we consider these further beginning with cell size.

669 The relationship between cell size and growth rate has long been of interest in the study of
 670 bacterial physiology, particularly following the now six decade-old observation that cell volume
 671 appears to increase exponentially with growth rate; known as Schaechter's growth law (*Schaechter
 et al., 1958; Taheri-Araghi et al., 2015*). Wild-type *E. coli* growing at relatively fast growth rates
 673 exhibit a remarkably constant cell cycle time t_{cyc} (referring to the C and D periods of DNA replication
 674 and cell division, respectively), as shown in **Figure 10(A)** for the data reproduced from (*Si et al.,
 675 2017*). With a constant cell cycle time, the exponential scaling in size has long been considered
 676 a direct consequence of cells initiating replication at a constant volume per origin. However, the
 677 particular mechanism that governs this relationship, and even the question of whether the change
 678 in average cell size is truly exponential have remained under debate (*Si et al., 2017; Harris and
 Theriot, 2018*).

680 Since protein accounts for more than half of cellular dry mass (BNID: 104954, *Milo et al. (2010);
 681 Bremer and Dennis (2008); Basan et al. (2015)*, cell size will vary in proportion to how much protein
 682 is synthesized over the cell cycle. Through our estimates in the sections on the central dogma, it is
 683 apparent that the processes of transcription (i.e. synthesis of mRNA) and translation are unlikely
 684 limiting steps in doubling the cell mass. In both cases, there is an overabundance of the requisite
 685 protein complexes (DNA and RNA polymerase, respectively) and there are mechanisms by which
 686 these synthesis processes can be parallelized. Therefore, the total protein mass is determined by
 687 $r_i \times R$ and the doubling time τ . The relationship between cell size and growth rate, however, will
 688 depend only on how the cell scales its ribosomal fraction Φ_R , as highlighted by **Equation 3**.

689 Ribosomal Abundance Defines Exponential Scaling Between Cell Size and Growth Rate
 690 A naïve strategy to increase growth rate given the constraint prescribed by **Equation 3**, would be
 691 to simply generate more ribosomes. In reality, large swaths of the proteome increases in absolute
 692 abundance at faster growth (Supplemental Figure X). Substantial empirical evidence has revealed
 693 a linear scaling between cell size (volume) and the number of chromosomal origins of replication,
 694 $\langle \# \text{ori} \rangle$, which is robust to a remarkable array of perturbations (*Si et al., 2017*). The number of
 695 origins $\langle \# \text{ori} \rangle$ is determined by how often replication must be initiated per cell doubling to maintain
 696 steady-state growth. This quantity can be approximately quantified via

$$\langle \# \text{ori} \rangle \approx 2^{\tau_{cyc}/\tau}, \quad (4)$$

697 where τ is the doubling time. In **Figure 10(A)**, we show the measurements of *Si et al. (2017)* for
 698 wild-type *E. coli* cells in nutrient-limit growth regimes. Using this data, we estimated $\langle \# \text{ori} \rangle$ for
 699 each condition in the amalgamated proteomic datasets. (shown in **Figure 10(A)**) if rRNA otherwise
 700 becoming rate limited at fast growth, this strategy allows for a roughly linear increase in ribosomes
 701 copy number with $\langle \# \text{ori} \rangle$ as shown in **Figure 10(B)** for the proteomic data.

702 It is notable that the majority of ribosomal proteins and rRNA operons are found closer to the
 703 DNA origin. Since multiple rounds of DNA initiation will effectively skew gene dosage in favor of
 704 genes near the origin (*Scholz et al., 2019*), it suggests that cells increase $\langle \# \text{ori} \rangle$ as a means to skew
 705 the ribosomal fraction Φ_R . We were unaware, however, of whether the change in gene dosage at
 706 fast growth materializes at the proteomic level. In **Figure 10(D)** we show a running boxcar average
 707 (500 kbp window) of protein copy number as a function of each gene's transcriptional start site
 708 (**Figure 10(D)**). While the protein copy numbers of individual proteins can vary substantially across
 709 the entire chromosome, we nonetheless observe a bias in expression across the chromosome
 710 under fast growth conditions (dark blue lines). The dramatic change in protein copy number near
 711 the origin is primarily due to the increase in ribosomal protein expression. This trend is in contrast
 712 to slower growth conditions (yellow) where the average copy number is much more uniform across
 713 the length of the chromosome.

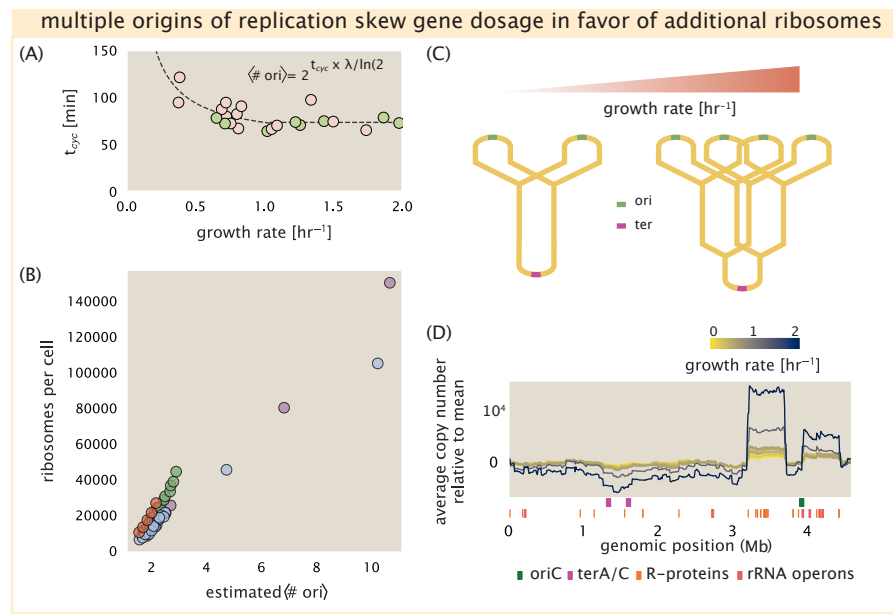


Figure 10. Multiple replication forks skew gene dosage and ribosomal content. (A) Experimental data from Si *et al.* (2017). Dashed line shows fit to the data, which were used to estimate $\langle \# \text{ori} \rangle$. t_{cyc} was assumed to vary in proportion to τ for doubling times great than 40 minutes, and then reach a minimum value of [fill in] minutes below this (see Supplemental Appendix X for additional details). Red data points correspond to measurements in strain MG1655, while light green points are for strain NCM3722. (B) Plot of the ribosome copy number estimated from the proteomic data against the estimated $\langle \# \text{ori} \rangle$ [NB: change to total protein abundance?]. (C) Schematic shows the expected increase in replication forks (or number of ori regions) as *E. coli* cells grow faster. (D) A running boxcar average of protein copy number is calculated for each each growth condition considered by (Schmidt *et al.*, 2016). A 0.5 Mb averaging window was used. Protein copy numbers are reported relative to their condition-specific means in order to center all data sets.

714 This result provides important evidence that although total protein content scales with $\langle \# \text{ ori} \rangle$, it
 715 is also the bias in gene dosage for genes closer to the origin that change the proteomic composition
 716 and allows an increase in the ribosomal fraction Φ_R at fast growth. For *E. coli*, we can then view
 717 the increase in ribosomal fraction Φ_R (and therefore, λ) as requiring a geometric increase in total
 718 protein abundance that is proportional to $\langle \# \text{ ori} \rangle$. This leads to an exponential increase in total
 719 protein mass (and cell size) as long as all ribosomes R are actively translating protein during cell
 720 doubling.

721 Growth in poor nutrient conditions.

722 While the above results suggest that it is the need to increase the number of ribosomes that sets an
 723 exponential scaling in cell size, this relationship is likely to falter at slow growth rates (below about
 724 0.5h^{-1}). In this regime ribosome copy number R no longer reflects the cell's protein synthesis ca-
 725 pacity. While cells appears to continue scaling R with $\langle \# \text{ ori} \rangle$ (*Figure 10(A)*), reaching a minimum
 726 ribosomal fraction of about 0.06, additional regulatory control through the small-molecule alar-
 727 mones (p)ppGpp reduces the fraction of actively translating ribosomes at slow growth (*Dai et al.,*
 728 *2016; Bosdriesz et al., 2015; Zhu and Dai, 2019*). In this section we consider the consequence of
 729 having excess ribosomes on maintaining steady-state growth in poor nutrient conditions.

730 The specific challenge lies in the ability of cells to maintain homeostasis when consumption
 731 of amino acids might exceed the rate of synthesis if all ribosomes were actively translating *Fig-*
 732 *ure 11A*. Without additional regulatory control, this would prevent continuous growth, and indeed
 733 for (p)ppGpp null strains, cells only grow in minimal media if additional amino acid supplements
 734 are present. In contrast, wild-type *E. coli* maintain a relatively high elongation rate even in station-
 735 ary phase ($\approx 8 \text{ AA/s}$, (*Dai et al., 2016, 2018*)).

736 Mitigation of translation activity helps maintain homeostasis in poor nutrient conditions
 737 To better understand how regulation of ribosomes influence growth rate in this slow growth regime
 738 we consider a coarse-grained model that relates elongation rate to a limiting supply of amino acids,
 739 which for simplicity we treat as a single, effective rate-limiting species. Under such a scenario, the
 740 elongation rate can be described as depending on the maximum elongation rate ($r_t^{\max} \approx 17.1 \text{ aa/s}$,
 741 (*Dai et al., 2016, 2018*)), an effective binding constant K_D between the pool of amino acids and their
 742 amino-acyl tRNAs, and the limiting amino acid concentration $[AA]_{eff}$.

$$r_t = r_t^{\max} \cdot \frac{1}{1 + K_D/[AA]_{eff}}. \quad (5)$$

743 For cells growing in minimal medium supplemented with glucose, the amino acid concentration
 744 is of order 100 mM (BNID: 110093, (*Milo et al., 2010; Bennett et al., 2009*)). To estimate K_D we
 745 note that for a growth rate of about 0.6 hr^{-1} *Dai et al. (2016)* measured an elongation rate of about
 746 12.5 amino acids per second, which gives $K_D \approx 40 \text{ mM}$. The maintenance of this amino acid pool
 747 $[AA]_{eff}$ will depend on the difference between the synthesis/supply rate of amino acids r_{AA} and
 748 consumption by ribosomes $r_t \times R \times f_a$, where we use f_a to account for the possible reduction of
 749 actively translating ribosomes (see Supplemental Appendix XX for further details on this model).

750 In *Figure 11(B)* we plot the growth rate and elongation rate as a function of the number of
 751 actively translating ribosomes. Growth rate is now determined by the active ribosomal fraction,

$$\lambda_{\text{translation-limited}} \approx \frac{r_t}{L_R} \Phi_R f_a. \quad (6)$$

752 If we consider constant values of amino acid synthesis rate r_{AA} (dashed lines) to reflect the avail-
 753 able parameter space for a specific growth condition, cells will grow fastest by maximizing their
 754 fraction of actively translating ribosomes. When we consider the experimental measurements
 755 from *Dai et al. (2018)* (yellow circles), which reflect growth in different nutrient conditions, we see
 756 that although cells reduce $R \times f_a$ in poorer nutrient conditions, they do so in a way that keeps

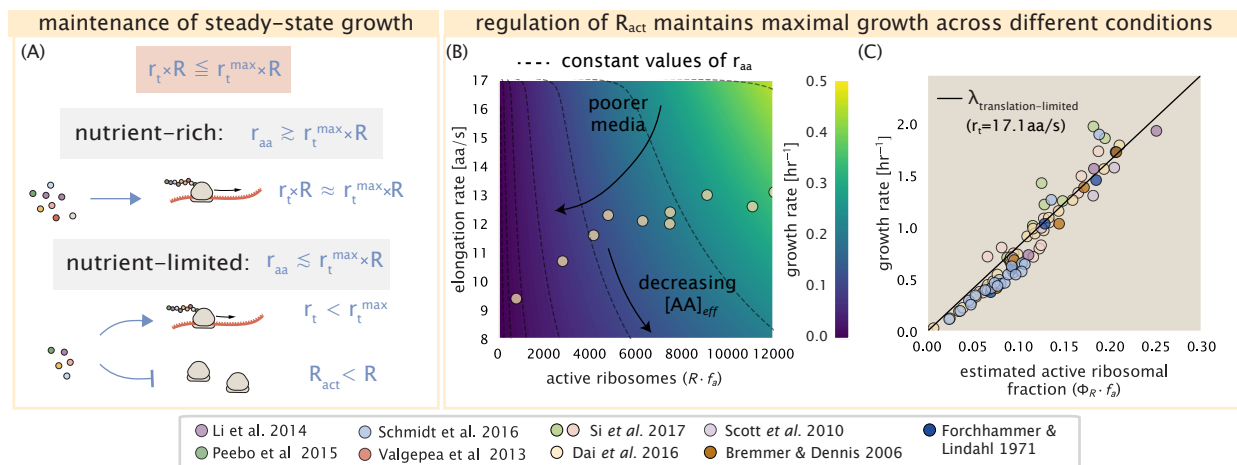


Figure 11. *E. coli* must regulate ribosomal activity in limiting nutrient conditions. (A) Schematic showing translation-specific requirements for maintenance of steady-state growth. In a nutrient rich environment, amino acid supply r_{aa} is sufficiently in excess of the demand by ribosomes translating at their maximal rate. In poorer nutrient conditions, reduced amino acid supply r_{aa} will decrease the rate of elongation. In a regime where r_{aa} is less than $r_t \cdot R$, the number of actively translating ribosomes will need to be reduced in order to maintain steady-state growth. (B) Translation elongation rate is plotted as a function of the number of actively translating ribosomes $R \cdot f_a$. Dashed lines correspond to a range of amino acid synthesis rates r_{aa} , from 10^3 to 10^6 . Growth rates are calculated according to Equation 1, assuming a constant ribosomal fraction of 8 percent. See appendix XX for additional details. (C) Experimental data from Dai *et al.* are used to estimate the fraction of actively translating ribosomes. The solid line represents the translation-limited growth rate for ribosomes elongating at 17.1 AA/s.

757 $[AA]_{eff}$ relatively constant. Given our estimate for the K_D of 40 mM, we would only expect a de-
758 crease from 100 mM to about 35 mM in the slowest growth conditions. While experimental data is
759 scarce, amino acid concentrations only decrease to about 60 mM for cells grown in minimal media
760 + acetate ($\lambda \approx 0.3 \text{ hr}^{-1}$ in our proteomic data) (Bennett *et al.*, 2009), qualitatively consistent with
761 our expectations. One explanation for the experimental data then is that the cell is regulating ribo-
762 some activity in order to maintain a sufficient pool of amino acids for growth. Any further increase
763 in $R \times f_a$ at constant r_{AA} would otherwise be associated with an additional drop in cellular amino
764 acids concentrations.

765 *E. coli* maximizes its steady-state growth rate by tuning both ribosomal content and trans-
766 lation activity.

767 Using the active fraction f_a measurements across a broad range of nutrient-limited growth condi-
768 tions from the work of Dai *et al.* (2016), we also estimated the active fraction of ribosomal protein
769 across our collated data (Figure 11(C)). Importantly, we find that across all growth conditions con-
770 sidered cells appear to maintain a growth rate consistent with Equation 3 with an elongation rate
771 of $r_t \approx 17.1 \text{ aa/s}$. While somewhat counter intuitive given that ribosomes translate at almost half
772 this rate in the poorest of growth conditions, it is because cells tune $r_t \times R \times f_a$ that they're able
773 to achieve these steady-state growth rates over such a broad range of conditions.

774 Recently it was shown that growth in a (p)ppGpp null strain abolishes both the scaling in cell
775 size and the $\langle \# \text{ ori} \rangle / \langle \# \text{ ter} \rangle$ ratio. Instead, cells exhibited a high $\langle \# \text{ ori} \rangle / \langle \# \text{ ter} \rangle$ closer to 4 and
776 cell size more consistent with a fast growth state where (p)ppGpp levels are low (Fernández-Coll
777 *et al.*, 2020) and ribosomal fraction is high (Zhu and Dai, 2019). This raises the possibility that
778 the action of (p)ppGpp is also mediating growth control and size scaling over this entire range of
779 growth conditions. Specifically, as nutrient conditions worsen, (p)ppGpp helps decrease multiple
780 rounds of DNA replication per cell doubling which effectively decreases both R and the total cell
781 size and in sufficiently poor growth conditions mitigates translation activity according to nutrient

782 availability.

783 References

- 784 Abelson, H., Johnson, L., Penman, S., and Green, H. (1974). Changes in RNA in relation to growth of the fibroblast:
 785 II. The lifetime of mRNA, rRNA, and tRNA in resting and growing cells. *Cell*, 1(4):161–165.
- 786 Aidelberg, G., Towbin, B. D., Rothschild, D., Dekel, E., Bren, A., and Alon, U. (2014). Hierarchy of non-glucose
 787 sugars in *Escherichia coli*. *BMC Systems Biology*, 8(1):133.
- 788 Antonenko, Y. N., Pohl, P., and Denisov, G. A. (1997). Permeation of ammonia across bilayer lipid membranes
 789 studied by ammonium ion selective microelectrodes. *Biophysical Journal*, 72(5):2187–2195.
- 790 Ashburner, M., Ball, C. A., Blake, J. A., Botstein, D., Butler, H., Cherry, J. M., Davis, A. P., Dolinski, K., Dwight, S. S.,
 791 Eppig, J. T., Harris, M. A., Hill, D. P., Ires-Tarver, L., Kasarskis, A., Lewis, S., Matese, J. C., Richardson, J. E.,
 792 Ringwald, M., Rubin, G. M., and Sherlock, G. (2000). Gene Ontology: tool for the unification of biology. *Nature Genetics*, 25(1):25–29.
- 793 Ason, B., Bertram, J. G., Hingorani, M. M., Beechem, J. M., O'Donnell, M., Goodman, M. F., and Bloom, L. B.
 794 (2000). A Model for *Escherichia coli* DNA Polymerase III Holoenzyme Assembly at Primer/Template Ends:
 795 DNA Triggers A Change In Binding Specificity of the γ Complex Clamp Loader. *Journal of Biological Chemistry*,
 796 275(4):3006–3015.
- 797 Assentoft, M., Kaptan, S., Schneider, H.-P., Deitmer, J. W., de Groot, B. L., and MacAulay, N. (2016). Aquaporin 4
 798 as a NH₃ Channel. *Journal of Biological Chemistry*, 291(36):19184–19195.
- 799 Basan, M., Zhu, M., Dai, X., Warren, M., Sévin, D., Wang, Y.-P., and Hwa, T. (2015). Inflating bacterial cells by
 800 increased protein synthesis. *Molecular Systems Biology*, 11(10):836.
- 801 Bauer, S. and Ziv, E. (1976). Dense growth of aerobic bacteria in a bench-scale fermentor. *Biotechnology and
 802 Bioengineering*, 18(1):81–94. _eprint: <https://onlinelibrary.wiley.com/doi/10.1002/bit.260180107>.
- 803 Belliveau, N. M., Barnes, S. L., Ireland, W. T., Jones, D. L., Sweredoski, M. J., Moradian, A., Hess, S., Kinney, J. B.,
 804 and Phillips, R. (2018). Systematic approach for dissecting the molecular mechanisms of transcriptional
 805 regulation in bacteria. *Proceedings of the National Academy of Sciences*, 115(21):E4796–E4805.
- 806 Bennett, B. D., Kimball, E. H., Gao, M., Osterhout, R., Van Dien, S. J., and Rabinowitz, J. D. (2009). Absolute
 807 metabolite concentrations and implied enzyme active site occupancy in *Escherichia coli*. *Nature Chemical
 808 Biology*, 5(8):593–599.
- 809 Birnbaum, L. S. and Kaplan, S. (1971). Localization of a Portion of the Ribosomal RNA Genes in *Escherichia coli*.
 810 *Proceedings of the National Academy of Sciences*, 68(5):925–929.
- 811 Booth, I. R., Mitchell, W. J., and Hamilton, W. A. (1979). Quantitative analysis of proton-linked transport systems.
 812 The lactose permease of *Escherichia coli*. *Biochemical Journal*, 182(3):687–696.
- 813 Bosdriesz, E., Molenaar, D., Teusink, B., and Bruggeman, F. J. (2015). How fast-growing bacteria robustly tune
 814 their ribosome concentration to approximate growth-rate maximization. *The FEBS Journal*, 282(10):2029–
 815 2044.
- 816 Bremer, H. and Dennis, P. P. (2008). Modulation of Chemical Composition and Other Parameters of the Cell at
 817 Different Exponential Growth Rates. *EcoSal Plus*, 3(1).
- 818 Browning, D. F. and Busby, S. J. W. (2016). Local and global regulation of transcription initiation in bacteria.
 819 *Nature Reviews Microbiology*, 14(10):638–650.
- 820 Cox, G. B., Newton, N. A., Gibson, F., Snoswell, A. M., and Hamilton, J. A. (1970). The function of ubiquinone in
 821 *Escherichia coli*. *Biochemical Journal*, 117(3):551–562.
- 822 Dai, X., Zhu, M., Warren, M., Balakrishnan, R., Okano, H., Williamson, J. R., Fredrick, K., and Hwa, T. (2018).
 823 Slowdown of Translational Elongation in *Escherichia coli* under Hyperosmotic Stress. - PubMed - NCBI. *mBio*,
 824 9(1):281.
- 825 Dai, X., Zhu, M., Warren, M., Balakrishnan, R., Patsalo, V., Okano, H., Williamson, J. R., Fredrick, K., Wang, Y.-P.,
 826 and Hwa, T. (2016). Reduction of translating ribosomes enables *Escherichia coli* to maintain elongation rates
 827 during slow growth. *Nature Microbiology*, 2(2):16231.
- 828 Escalante, A., Salinas Cervantes, A., Gosset, G., and Bolívar, F. (2012). Current knowledge of the *Escherichia coli*
 829 phosphoenolpyruvate-carbohydrate phosphotransferase system: Peculiarities of regulation and impact on
 830 growth and product formation. *Applied Microbiology and Biotechnology*, 94(6):1483–1494.

- 832 Feist, A. M., Henry, C. S., Reed, J. L., Krummenacker, M., Joyce, A. R., Karp, P. D., Broadbelt, L. J., Hatzimanikatis,
 833 V., and Palsson, B. Ø. (2007). A genome-scale metabolic reconstruction for *Escherichia coli* K-12 MG1655 that
 834 accounts for 1260 ORFs and thermodynamic information. *Molecular Systems Biology*, 3(1):121.
- 835 Fernández-Coll, L., Maciąg-Dorszynska, M., Tailor, K., Vadia, S., Levin, P. A., Szalewska-Palasz, A., Cashel, M.,
 836 and Dunny, G. M. (2020). The Absence of (p)ppGpp Renders Initiation of *Escherichia coli* Chromosomal DNA
 837 Synthesis Independent of Growth Rates. *mBio*, 11(2):45.
- 838 Fijalkowska, I. J., Schaaper, R. M., and Jonczyk, P. (2012). DNA replication fidelity in *Escherichia coli*: A multi-DNA
 839 polymerase affair. *FEMS Microbiology Reviews*, 36(6):1105–1121.
- 840 Finkelstein, I. J. and Greene, E. C. (2013). Molecular Traffic Jams on DNA. *Annual Review of Biophysics*, 42(1):241–
 841 263.
- 842 Gama-Castro, S., Salgado, H., Santos-Zavaleta, A., Ledezma-Tejeida, D., Muñiz-Rascado, L., García-Sotelo, J. S.,
 843 Alquicira-Hernández, K., Martínez-Flores, I., Pannier, L., Castro-Mondragón, J. A., Medina-Rivera, A., Solano-
 844 Lira, H., Bonavides-Martínez, C., Pérez-Rueda, E., Alquicira-Hernández, S., Porrón-Sotelo, L., López-Fuentes,
 845 A., Hernández-Koutoucheva, A., Moral-Chávez, V. D., Rinaldi, F., and Collado-Vides, J. (2016). RegulonDB
 846 version 9.0: High-level integration of gene regulation, coexpression, motif clustering and beyond. *Nucleic
 847 Acids Research*, 44(D1):D133–D143.
- 848 Ge, J., Yu, G., Ator, M. A., and Stubbe, J. (2003). Pre-Steady-State and Steady-State Kinetic Analysis of *E. coli* Class
 849 I Ribonucleotide Reductase. *Biochemistry*, 42(34):10071–10083.
- 850 Godin, M., Delgado, F. F., Son, S., Grover, W. H., Bryan, A. K., Tzur, A., Jorgensen, P., Payer, K., Grossman, A. D.,
 851 Kirschner, M. W., and Manalis, S. R. (2010). Using buoyant mass to measure the growth of single cells. *Nature
 852 Methods*, 7(5):387–390.
- 853 Goldman, S. R., Nair, N. U., Wells, C. D., Nickels, B. E., and Hochschild, A. (2015). The primary σ factor in *Es-
 854 cherichia coli* can access the transcription elongation complex from solution *in vivo*. *eLife*, 4:e10514.
- 855 Harris, L. K. and Theriot, J. A. (2018). Surface Area to Volume Ratio: A Natural Variable for Bacterial Morphogen-
 856 esis. *Trends in microbiology*, 26(10):815–832.
- 857 Harris, R. M., Webb, D. C., Howitt, S. M., and Cox, G. B. (2001). Characterization of PitA and PitB from *Escherichia
 858 coli*. *Journal of Bacteriology*, 183(17):5008–5014.
- 859 Heldal, M., Norland, S., and Tumyr, O. (1985). X-ray microanalytic method for measurement of dry matter and
 860 elemental content of individual bacteria. *Applied and Environmental Microbiology*, 50(5):1251–1257.
- 861 Henkel, S. G., Beek, A. T., Steinsiek, S., Stagge, S., Bettenbrock, K., de Mattos, M. J. T., Sauter, T., Sawodny, O.,
 862 and Ederer, M. (2014). Basic Regulatory Principles of *Escherichia coli*'s Electron Transport Chain for Varying
 863 Oxygen Conditions. *PLoS ONE*, 9(9):e107640.
- 864 Ingledew, W. J. and Poole, R. K. (1984). The respiratory chains of *Escherichia coli*. *Microbiological Reviews*,
 865 48(3):222–271.
- 866 Ireland, W. T., Beeler, S. M., Flores-Bautista, E., Belliveau, N. M., Sweredoski, M. J., Moradian, A., Kinney, J. B.,
 867 and Phillips, R. (2020). Deciphering the regulatory genome of *Escherichia coli*, one hundred promoters at a
 868 time. *bioRxiv*.
- 869 Jacob, F. and Monod, J. (1961). Genetic regulatory mechanisms in the synthesis of proteins. *Journal of Molecular
 870 Biology*, 3(3):318–356.
- 871 Jensen, R. B., Wang, S. C., and Shapiro, L. (2001). A moving DNA replication factory in *Caulobacter crescentus*.
 872 *The EMBO Journal*, 20(17):4952–4963.
- 873 Jun, S., Si, F., Pugatch, R., and Scott, M. (2018). Fundamental principles in bacterial physiology - history, recent
 874 progress, and the future with focus on cell size control: A review. *Reports on Progress in Physics*, 81(5):056601.
- 875 Kapanidis, A. N., Margeat, E., Laurence, T. A., Doose, S., Ho, S. O., Mukhopadhyay, J., Kortkhonjia, E., Mekler, V.,
 876 Ebright, R. H., and Weiss, S. (2005). Retention of Transcription Initiation Factor Σ 70 in Transcription Elonga-
 877 tion: Single-Molecule Analysis. *Molecular Cell*, 20(3):347–356.
- 878 Khademi, S., O'Connell, J., Remis, J., Robles-Colmenares, Y., Miercke, L.J.W., and Stroud, R. M. (2004). Mechanism
 879 of Ammonia Transport by Amt/MEP/Rh: Structure of AmtB at 1.35 Å. *Science*, 305(5690):1587–1594.

- 880 Khademian, M. and Imlay, J. A. (2017). *Escherichia coli* cytochrome c peroxidase is a respiratory oxidase that
881 enables the use of hydrogen peroxide as a terminal electron acceptor. *Proceedings of the National Academy
882 of Sciences*, 114(33):E6922–E6931.
- 883 Li, G.-W., Burkhardt, D., Gross, C., and Weissman, J. S. (2014). Quantifying absolute protein synthesis rates
884 reveals principles underlying allocation of cellular resources. *Cell*, 157(3):624–635.
- 885 Liu, M., Durfee, T., Cabrera, J. E., Zhao, K., Jin, D. J., and Blattner, F. R. (2005). Global Transcriptional Programs
886 Reveal a Carbon Source Foraging Strategy by *Escherichia coli*. *Journal of Biological Chemistry*, 280(16):15921–
887 15927.
- 888 Lu, D., Grayson, P., and Schulten, K. (2003). Glycerol Conductance and Physical Asymmetry of the *Escherichia
889 coli* Glycerol Facilitator GlpF. *Biophysical Journal*, 85(5):2977–2987.
- 890 Lynch, M. and Marinov, G. K. (2015). The bioenergetic costs of a gene. *Proceedings of the National Academy of
891 Sciences*, 112(51):15690–15695.
- 892 Maaløe, O. (1979). *Regulation of the Protein-Synthesizing Machinery—Ribosomes, tRNA, Factors, and So On. Gene
893 Expression*. Springer.
- 894 Milo, R., Jorgensen, P., Moran, U., Weber, G., and Springer, M. (2010). BioNumbers—the database of key num-
895 bers in molecular and cell biology. *Nucleic Acids Research*, 38(suppl_1):D750–D753.
- 896 Monod, J. (1947). The phenomenon of enzymatic adaptation and its bearings on problems of genetics and
897 cellular differentiation. *Growth Symposium*, 9:223–289.
- 898 Mooney, R. A., Darst, S. A., and Landick, R. (2005). Sigma and RNA Polymerase: An On-Again, Off-Again Rela-
899 tionship? *Molecular Cell*, 20(3):335–345.
- 900 Mooney, R. A. and Landick, R. (2003). Tethering Σ 70 to RNA polymerase reveals high *in vivo* activity of σ factors
901 and Σ 70-dependent pausing at promoter-distal locations. *Genes & Development*, 17(22):2839–2851.
- 902 Neidhardt, F. C., Ingraham, J., and Schaechter, M. (1991). *Physiology of the Bacterial Cell - A Molecular Approach*,
903 volume 1. Elsevier.
- 904 Ojkic, N., Serbanescu, D., and Banerjee, S. (2019). Surface-to-volume scaling and aspect ratio preservation in
905 rod-shaped bacteria. *eLife*, 8:642.
- 906 Patrick, M., Dennis, P. P., Ehrenberg, M., and Bremer, H. (2015). Free RNA polymerase in *Escherichia coli*.
907 *Biochimie*, 119:80–91.
- 908 Peebo, K., Valgepea, K., Maser, A., Nahku, R., Adamberg, K., and Vilu, R. (2015). Proteome reallocation in *Es-
909 cherichia coli* with increasing specific growth rate. *Molecular BioSystems*, 11(4):1184–1193.
- 910 Perdue, S. A. and Roberts, J. W. (2011). σ^{70} -dependent Transcription Pausing in *Escherichia coli*. *Journal of
911 Molecular Biology*, 412(5):782–792.
- 912 Phillips, R. (2018). Membranes by the Numbers. In *Physics of Biological Membranes*, pages 73–105. Springer,
913 Cham, Cham.
- 914 Ramos, S. and Kaback, H. R. (1977). The relation between the electrochemical proton gradient and active trans-
915 port in *Escherichia coli* membrane vesicles. *Biochemistry*, 16(5):854–859.
- 916 Rosenberg, H., Gerdes, R. G., and Chegwidden, K. (1977). Two systems for the uptake of phosphate in *Escherichia
917 coli*. *Journal of Bacteriology*, 131(2):505–511.
- 918 Rudd, S. G., Valerie, N. C. K., and Helleday, T. (2016). Pathways controlling dNTP pools to maintain genome
919 stability. *DNA Repair*, 44:193–204.
- 920 Sánchez-Romero, M. A., Molina, F., and Jiménez-Sánchez, A. (2011). Organization of ribonucleoside diphosphate
921 reductase during multifork chromosome replication in *Escherichia coli*. *Microbiology*, 157(8):2220–2225.
- 922 Schaechter, M., Maaløe, O., and Kjeldgaard, N. O. (1958). Dependency on Medium and Temperature of Cell Size
923 and Chemical Composition during Balanced Growth of *Salmonella typhimurium*. *Microbiology*, 19(3):592–606.
- 924 Schmidt, A., Kochanowski, K., Vedelaar, S., Ahrné, E., Volkmer, B., Callipo, L., Knoops, K., Bauer, M., Aebersold,
925 R., and Heinemann, M. (2016). The quantitative and condition-dependent *Escherichia coli* proteome. *Nature
926 Biotechnology*, 34(1):104–110.

- 927 Scholz, S. A., Diao, R., Wolfe, M. B., Fivenson, E. M., Lin, X. N., and Freddolino, P. L. (2019). High-Resolution
928 Mapping of the *Escherichia coli* Chromosome Reveals Positions of High and Low Transcription. *Cell Systems*,
929 8(3):212–225.e9.
- 930 Scott, M., Gunderson, C. W., Mateescu, E. M., Zhang, Z., and Hwa, T. (2010). Interdependence of cell growth and
931 gene expression: origins and consequences. *Science*, 330(6007):1099–1102.
- 932 Sekowska, A., Kung, H.-F., and Danchin, A. (2000). Sulfur Metabolism in *Escherichia coli* and Related Bacteria:
933 Facts and Fiction. *Journal of Molecular Microbiology and Biotechnology*, 2(2):34.
- 934 Shi, H., Bratton, B. P., Gitai, Z., and Huang, K. C. (2018). How to Build a Bacterial Cell: MreB as the Foreman of
935 *E. coli* Construction. *Cell*, 172(6):1294–1305.
- 936 Si, F., Le Treut, G., Sauls, J. T., Vadia, S., Levin, P. A., and Jun, S. (2019). Mechanistic Origin of Cell-Size Control
937 and Homeostasis in Bacteria. *Current Biology*, 29(11):1760–1770.e7.
- 938 Si, F., Li, D., Cox, S. E., Sauls, J. T., Azizi, O., Sou, C., Schwartz, A. B., Erickstad, M. J., Jun, Y., Li, X., and Jun, S. (2017).
939 Invariance of Initiation Mass and Predictability of Cell Size in *Escherichia coli*. *Current Biology*, 27(9):1278–1287.
- 940 Sirko, A., Zatyka, M., Sadowy, E., and Hulanicka, D. (1995). Sulfate and thiosulfate transport in *Escherichia coli* K-
941 12: Evidence for a functional overlapping of sulfate- and thiosulfate-binding proteins. *Journal of Bacteriology*,
942 177(14):4134–4136.
- 943 Stasi, R., Neves, H. I., and Spira, B. (2019). Phosphate uptake by the phosphonate transport system PhnCDE.
944 *BMC Microbiology*, 19.
- 945 Stevenson, B. S. and Schmidt, T. M. (2004). Life History Implications of rRNA Gene Copy Number in *Escherichia*
946 *coli*. *Applied and Environmental Microbiology*, 70(11):6670–6677.
- 947 Stouthamer, A. H. (1973). A theoretical study on the amount of ATP required for synthesis of microbial cell
948 material. *Antonie van Leeuwenhoek*, 39(1):545–565.
- 949 Stouthamer, A. H. and Bettenhausen, C. W. (1977). A continuous culture study of an ATPase-negative mutant
950 of *Escherichia coli*. *Archives of Microbiology*, 113(3):185–189.
- 951 Svenningsen, S. L., Kongstad, M., Stenum, T. S. n., Muñoz-Gómez, A. J., and Sørensen, M. A. (2017). Transfer RNA
952 is highly unstable during early amino acid starvation in *Escherichia coli*. *Nucleic Acids Research*, 45(2):793–804.
- 953 Szenk, M., Dill, K. A., and de Graff, A. M. R. (2017). Why Do Fast-Growing Bacteria Enter Overflow Metabolism?
954 Testing the Membrane Real Estate Hypothesis. *Cell Systems*, 5(2):95–104.
- 955 Taheri-Araghi, S., Bradde, S., Sauls, J. T., Hill, N. S., Levin, P. A., Paulsson, J., Vergassola, M., and Jun, S. (2015).
956 Cell-size control and homeostasis in bacteria. - PubMed - NCBI. *Current Biology*, 25(3):385–391.
- 957 Tatusov, R. L., Galperin, M. Y., Natale, D. A., and Koonin, E. V. (2000). The COG database: a tool for genome-scale
958 analysis of protein functions and evolution. *Nucleic Acids Research*, 28(1):33–36.
- 959 Taymaz-Nikerel, H., Borujeni, A. E., Verheijen, P. J. T., Heijnen, J. J., and van Gulik, W. M. (2010).
960 Genome-derived minimal metabolic models for *Escherichia coli* mg1655 with estimated in vivo
961 respiratory ATP stoichiometry. *Biotechnology and Bioengineering*, 107(2):369–381. _eprint:
962 <https://onlinelibrary.wiley.com/doi/pdf/10.1002/bit.22802>.
- 963 The Gene Ontology Consortium (2018). The Gene Ontology Resource: 20 years and still GOing strong. *Nucleic
964 Acids Research*, 47(D1):D330–D338.
- 965 Valgepea, K., Adamberg, K., Seiman, A., and Vilu, R. (2013). *Escherichia coli* achieves faster growth by increasing
966 catalytic and translation rates of proteins. *Molecular BioSystems*, 9(9):2344.
- 967 van Heeswijk, W. C., Westerhoff, H. V., and Boogerd, F. C. (2013). Nitrogen Assimilation in *Escherichia coli*: Putting
968 Molecular Data into a Systems Perspective. *Microbiology and Molecular Biology Reviews*, 77(4):628–695.
- 969 Weber, J. and Senior, A. E. (2003). ATP synthesis driven by proton transport in F1FO-ATP synthase. *FEBS Letters*,
970 545(1):61–70.
- 971 Willsky, G. R., Bennett, R. L., and Malamy, M. H. (1973). Inorganic Phosphate Transport in *Escherichia coli*: Involvement
972 of Two Genes Which Play a Role in Alkaline Phosphatase Regulation. *Journal of Bacteriology*, 113(2):529–
973 539.

- 974 Zhang, L., Jiang, W., Nan, J., Almqvist, J., and Huang, Y. (2014a). The *Escherichia coli* CysZ is a pH dependent sulfate
975 transporter that can be inhibited by sulfite. *Biochimica et Biophysica Acta (BBA) - Biomembranes*, 1838(7):1809–
976 1816.
- 977 Zhang, Z., Aboulwafa, M., and Saier, M. H. (2014b). Regulation of crp gene expression by the catabolite repres-
978 sor/activator, cra, in *Escherichia coli*. *Journal of Molecular Microbiology and Biotechnology*, 24(3):135–141.
- 979 Zhu, M. and Dai, X. (2019). Growth suppression by altered (p)ppGpp levels results from non-optimal resource
980 allocation in *Escherichia coli*. *Nucleic Acids Research*, 47(9):4684–4693.